Rapid Determination of Pavement Moduli with Spectral-Analysis-of-Surface-Waves Method

by

Soheil Nazarian, Ph.D., P.E.

Deren Yuan, Ph.D.

and

Mark R. Baker, Ph.D.

Research Project 0-1243

Automated Equipment for Characterizing the Properties
and Thicknesses of Pavement Layers

Conducted for

Texas Department of Transportation
in cooperation with
Federal Highway Administration

The Center for Geotechnical and Highway Materials Research
The University of Texas at El Paso
El Paso, TX 79968-0516

Research Report 1243-1
November, 1995

TECHNICAL REPORT STANDARD TITLE PAGE

1. Report No.	2. Government Accession No.	3. Recipient's Catalog No.
TX-94 1243-1		

4. Title and Subtitle	5. Report Date
Rapid Determination of Moduli with Spectral-Analysis-of-Surface-Waves Method	November, 1995
	6. Performing Organization Code

7. Author(s)	8. Performing Organization Report No.
Nazarian S., Yuan D., and Baker M.R.	Research Report 1243-1

9. Performing Organization Name and Address	10. Work Unit No.
Center for Geotechnical and Highway Materials Research The University of Texas at El Paso El Paso, Texas 79968-0516	11. Contract or Grant No. Study No. 0-1243

12. Sponsoring Agency Name and Address	13. Type of Report and Period Covered
Texas Department of Transportation P.O. Box 5080 Austin, Texas 78763	Final Report Sept. 1, 1989-Aug 31, 1994
	14. Sponsoring Agency Code

15. Supplementary Notes

Research Performed in Cooperation with TxDOT and FHWA
Research Study Title: Automated Equipment for Characterizing the Properties and Thicknesses of Pavement Layers

16. Abstract

The Spectral-Analysis-of-Surface-Waves (SASW) method has been used as a nondestructive test method for determining elastic modulus profiles of pavement systems. To implement the method in day-to-day activities of any pavement evaluation program, three steps are necessary. First, field data acquisition should be carried out rapidly. This has been achieved by utilizing a newly-developed device called the Seismic Pavement Analyzer (patent pending). Second, the raw data should be manipulated to a dispersion curve in an automated manner. An algorithm has been developed which can perform this task. The last step is to determine the elastic modulus of different layers from the dispersion curve. A backcalculation technique based upon the generalized inverse theory is developed. The technique provides a fast and automated procedure for simultaneously determining moduli and thickness of pavements. In addition, some description of uncertainty in the backcalculated results is provided.

In this report, the development of these algorithms are discussed. The speed and accuracy as well as the limitations of the algorithms are demonstrated. Several actual field case histories are included to exhibit the usefulness of the method in actual field testing.

17. Key Words	18. Distribution Statement
Modulus, Nondestructive Testing, Seismic Methods, Resilient Modulus, SASW Method, Seismic Pavement Analyzer	No restrictions. This document is available to the public through the National Technical Information Service, 5285 Port Royal Road, Springfield, Virginia 22161

19. Security Classif. (of this report)	20. Security Classif. (of this page)	21. No. of Pages	22. Price
Unclassified	Unclassified	76	

Form DOT F 1700.7 (8-69)

NOT INTENDED FOR CONSTRUCTION, BIDDING, OR PERMIT PURPOSES

Soheil Nazarian, Ph.D., P.E. (69263)
Rafael Pezo, Ph.D.
Miguel Picornell, Ph.D.

Acknowledgements

The authors would like to give their sincere appreciation to Robert C. Briggs, Jeff Demon Jackson, and Mark McDaniel of the TxDOT Design Division for their support. Thanks are also due to all personnel of the Pavement Evaluation Group, especially Carl Bertrand.

Abstract

The Spectral-Analysis-of-Surface-Waves (SASW) method has been used as a nondestructive test method for determining elastic modulus profiles of pavement systems. To perform the test, a disturbance is applied to the pavement surface to generate stress waves which propagate mostly as surface waves of various wavelengths. The waves are monitored and captured with a data acquisition system. Signal and spectral analyses are utilized to determine a dispersion curve (variation in phase velocity with wavelength).

To implement the method in day-to-day activities of any pavement evaluation program, three steps are necessary. First, field data acquisition should be carried out rapidly. This has been achieved by utilizing a newly-developed device called the Seismic Pavement Analyzer (patent pending).

Second, the raw data should be manipulated to a dispersion curve in an automated manner. An algorithm has been developed which can perform this task.

The last step is to determine the elastic modulus of different layers from the dispersion curve. Several alternatives are available. First, trial and error (forward modelling) process can be carried out. Second, optimization techniques can be utilized. Finally, generalized inverse theory can be implemented. In most applications, the backcalculation of layer moduli is accomplished using a manual trial and error matching process between the theoretical and experimental dispersion curves. Unfortunately, this process is rather time-consuming and requires engineering judgment. To improve this aspect of SASW testing, a backcalculation technique based upon the generalized inverse theory is developed. The technique provides a fast and automated procedure for simultaneously determining layer elastic moduli and thickness of pavements. In addition, some description of uncertainty in the backcalculated results is provided.

In this report, the development of these algorithms are discussed. The speed and accuracy as well as the limitations of the algorithms are demonstrated. Several actual field case histories are included to exhibit the usefulness of the method in actual field testing.

Implementation Statement

At this time the implementation of the results from this study is quite possible. A prototype Seismic Pavement Analyzer (SPA) has been delivered to TxDOT. The software packages necessary are also provided. In our opinion, the findings should be immediately implemented on trial basis so that the possible logistical and practical problems with the device and algorithms can be addressed.

Table of Contents

List of Figures

List of Tables

Chapter 1

Introduction

As a nondestructive test (NDT) method, the Spectral Analysis of Surface Waves (SASW) method has been used to determine elastic modulus profiles of pavements. The SASW method is based upon the dispersion property of seismic surface waves of Rayleigh type in layered media. A complete SASW test includes three major steps: 1) field testing, 2) determination of experimental dispersion curve, and 3) determination of stiffness profile.

The in situ testing consists of generating and detecting surface waves by impacting the surface of the pavement and monitoring and capturing the motion of the pavement surface at several points. The captured signals are manipulated utilizing the Fourier and spectral analyses to determine the cross power spectra and the coherence functions.

Determination of the experimental dispersion curve consists of processing the cross power spectra and the coherence functions. This curve represents the dependence of Rayleigh wave phase velocity on frequency or wavelength.

Determining the elastic modulus profile from the experimental dispersion curve is the last but the most time-consuming and complicated step. This process is known as backcalculation or inversion. To accomplish this task, a manual trial and error (forward modelling) procedure has been successfully employed for years. A merit of the forward modelling procedure is that all common sense notions can be incorporated in the trial and error stage. This, however, implies that a fairly experienced person is needed to conduct this task efficiently. Therefore, one of the major shortcomings with the procedure is probably the time required to reduce the data. To remedy this shortcoming, an automated procedure is desirable.

Scope of Work

To turn the SASW method to a practical testing method, all aspects of the method such as data collection, data reduction, and data analysis should be automated. A device, the Seismic Pavement Analyzer, for conducting the field tests rapidly (in about one minute) has been development for SHRP at UTEP. One prototype of the device has been constructed for TxDOT.

An algorithm for automatically determining the experimental dispersion curve has been coded. The automation of this step significantly reduces the data reduction efforts.

Finally, a backcalculation process has been developed and is described in this report. The process, which is based upon the general inverse theory, provides an automated iterative algorithm for rapidly determining modulus profiles from dispersion curves. At the same time, the process may yield information needed for uncertainty analysis of backcalculated results. Synthetic (theoretically-derived) data and actual case studies are included to illustrate some aspects of the strengths and limitations of the process.

Organization

As an introductory effort, Chapter 2 contains a review of literature. In Chapter 3, the methodology adopted for the construction of experimental dispersion curves from field data is described. The process followed to compute theoretical dispersion curves and a brief description of the dispersion characteristic for pavements are contained in Chapter 4. In Chapter 5, the inversion technique utilized is discussed. The capabilities of the Seismic Pavement Analyzer are described in Chapter 6. Finally, example case studies are included in Chapter 7 to demonstrate the practical uses of the device. Chapter 8 is the closure which contains the summary and conclusions of this research effort.

Chapter 2

Background

Historical Development

The early developments of the surface wave method for use in the civil engineering field is summarized by Nazarian (1984). The initial experimental developments have been attributed to the German Society of Soil Mechanics, the U.S. Army Corps of Engineers (Fry, 1965) and Jones (1958). Jones (1958) also proposed an analytical method for data reduction. Heisey (1982) studied the feasibility of utilizing transient signals to construct dispersion curves.

The major ground work for the SASW method has been laid in the last 15 years. Nazarian and Stokoe (1986, 1987) developed the experimental and theoretical aspects of the SASW method as applied to geotechnical and pavement engineering fields. They developed the suitable method for conducting the test in situ. They also developed a computer algorithm named INVERT (Nazarian, 1984) for determining the stiffness profile from a dispersion curve.

In the last ten years, much effort has been focused on improving different aspects of the SASW tests. Drnevich et al. (1985) successfully utilized a vibrator connected to a random function generator as a source. Sanchez-Salinero et al. (1987) analytically studied the most feasible source-receiver configuration. They indicated that a desirable distance between the source and the first receiver is equal to the distance between the adjacent receivers. Sheu et al (1987) recommended that, for the set-up suggested by Sanchez-Salinero et al. (1987), wavelengths greater than three times the distance between the receivers should not be considered. Hiltunen (1988) experimentally confirmed this recommendation.

Rix (1988), based upon an experimental investigation, concluded that typically most of the surface wave energy in SASW testing is associated with the fundamental mode of vibration. Hossain and Drnevich (1989) presented an algorithm for determination of stiffness profile. Optimization techniques were used to automate the inversion process. They applied the algorithm to synthetic dispersion data with success. Gucunski and Woods (1991) conducted an analytical study to quantify some of the problems associated with the alternative soft and hard layers.

Barker and Stevens (1991) report some of the precautions which should be considered during the processing of the SASW field data. Satoh et al. (1991) described an approximate method for collection and reduction of data. However, the method has limited application except in very uniform and simple soil profiles.

Desai (1991) proposed a rapid method for constructing dispersion curves from the data measured in the field.

Rix and Leipski (1991) discussed an inversion process for soil sites. Foinquinos (1991) presented a simplified least-squares minimization routine for inversion of surface wave data. He also compared the layered solution with an axisymmetric solution where the effects of body waves are considered. Even though the axisymmetric full wave solution is valuable in understanding the shortcomings of the SASW method, it has limited use in actual site investigation because of the computation time involved.

In the development of surface wave theory and methods, much attention has been paid to the situation where stiffness increases with depth. This well-studied situation covers most geological and geotechnical systems. In this case, the dispersion of surface waves is known as the normal dispersion for which the phase velocity in general increases continuously with wavelength. For the normal dispersion, the phase velocity of each excitation mode is uniquely defined, and, at least for the first few modes, can be accurately computed at any frequency of interest without difficulty.

In comparison with the above situation, the dispersion of Rayleigh waves (or generalized Rayleigh waves) in a layered system of pavement type where stiffness or shear wave velocity decreases with depth (at least in a depth range of interest) is more complicated. This is referred to as the inverse or abnormal dispersion against the normal dispersion. For the abnormal dispersion, the secular equation of dispersion is in general complex. This is mathematically analogous to the so-called leaky mode. In this case, the dispersion field of single mode may consist of multiple segments or branches and, thus, wave velocity is no longer a continuous function of frequency or wavelength. This feature has been shown in the results obtained from different analysis approaches (Jones, 1962; Vidale, 1964; and Nazarian, 1984). The branches of a dispersion curve contain the explicit information about layering, and characteristic shear and compressional wave velocities of a layered system. It is expected that if the branches in an experimental dispersion curve are well defined, the layer properties of the system can be closely determined. In particular, this feature is of great importance to developing the SASW method into a standard tool for pavement evaluation.

The ultimate goal of SASW testing at a site is to provide a velocity or modulus profile through an inversion process which minimizes (under certain criteria) the difference between the experimental dispersion curve and the calculated one from a trial profile. In many cases, however, the branches in an experimental dispersion curve are not easy to identify, although some examples have been reported (e.g., Jones, 1962, and Vidale, 1964). This is mainly for three reasons: 1) heterogeneity of layers in a pavement, 2) effect of reflection, and 3) use of filtering and averaging processes in data reduction. Thus, one usually has to face a difficulty that is how to match a theoretical dispersion curve with branches or discontinuities with a smooth experimental dispersion curve. The situation can become more critical when inversion

is carried out through an automated iteration procedure. To deal with the problem, a knowledge of the theoretical dispersion characteristic for typical pavement structures is desirable.

In order to make the SASW method practical, two simplifying assumptions have been made in the method. First, it is assumed that the structure of a pavement can be approximated by a stack of horizontal layers and that the material properties of each layer are constant. Second, it is assumed that only the plane Rayleigh waves are involved. The effect of (uncoupled) body waves is ignored. The validity of this assumption has been evaluated by Sanchez-Salinero (1987) in an analytical study and by Rix et al. (1991) in an experimental study. The results from these studies show that the effect of ignoring body waves is quite minor as long as the source-receiver geometry relative to the wavelength is kept within certain limits. With this assumption, however, the inversion of the SASW data for composite pavements is not possible.

Testing Procedure

The main goal in performing the SASW in the field is to obtain an experimental dispersion curve. Two spectral functions, the cross power spectrum and the coherence function, are utilized for this task.

A schematic diagram of SASW testing setup used for measuring these two functions is shown in Fig. 2.1. To perform a test in the field, several steps should be taken (Nazarian and Stokoe, 1986). An imaginary centerline for the receiver array is selected. Two or more receivers are then placed on the ground surface an equal distance from the centerline. A disturbance is applied to the ground surface, and a group of surface waves of various frequencies are generated in the medium. The records are monitored, captured and saved for further reduction. After the testing is complete, the receivers are kept in their original positions, but the source is moved to the opposite side of the imaginary centerline and testing is repeated. This process is named as the reversing of the profile.

Nazarian and Stokoe (1986) found that, to maximize the quality of the experimental dispersion curve, a common receiver midpoint (CRMP) array is the most appropriate (see Fig. 2.2a). In CRMP geometry, an imaginary center line is selected between the two receivers. The two receivers are moved away from the imaginary centerline at an equal pace, and the source is moved such that the distance between the source and near receiver is equal to the distance between the two receivers. However, as Hiltunen and Woods (1990) pointed out, the common source (Fig. 2.2b) geometry would be more appropriate for automation. They demonstrated that with small sacrifice in the quality, the testing process would be significantly shortened with the common source array.

The cross power spectrum between two signals captured by two receivers is used to obtain the relative phase shift at each frequency. This phase shift can be translated into travel time. Construction of experimental dispersion curves from the phase information is described in detail in Chapters 3.

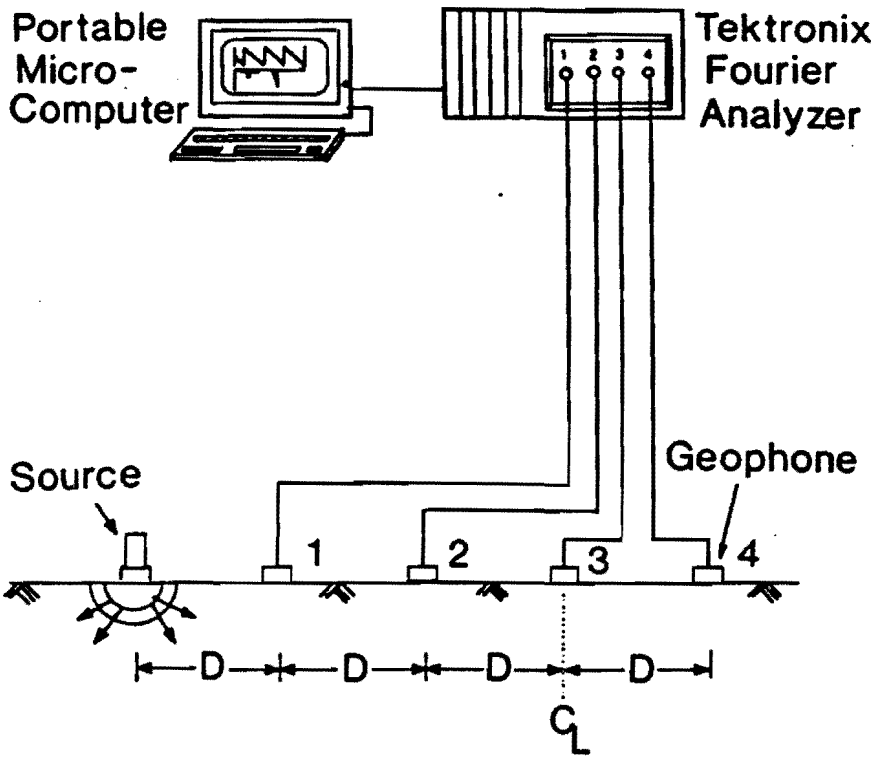

Fig. 2.1 - A schematic diagram of SASW testing setup

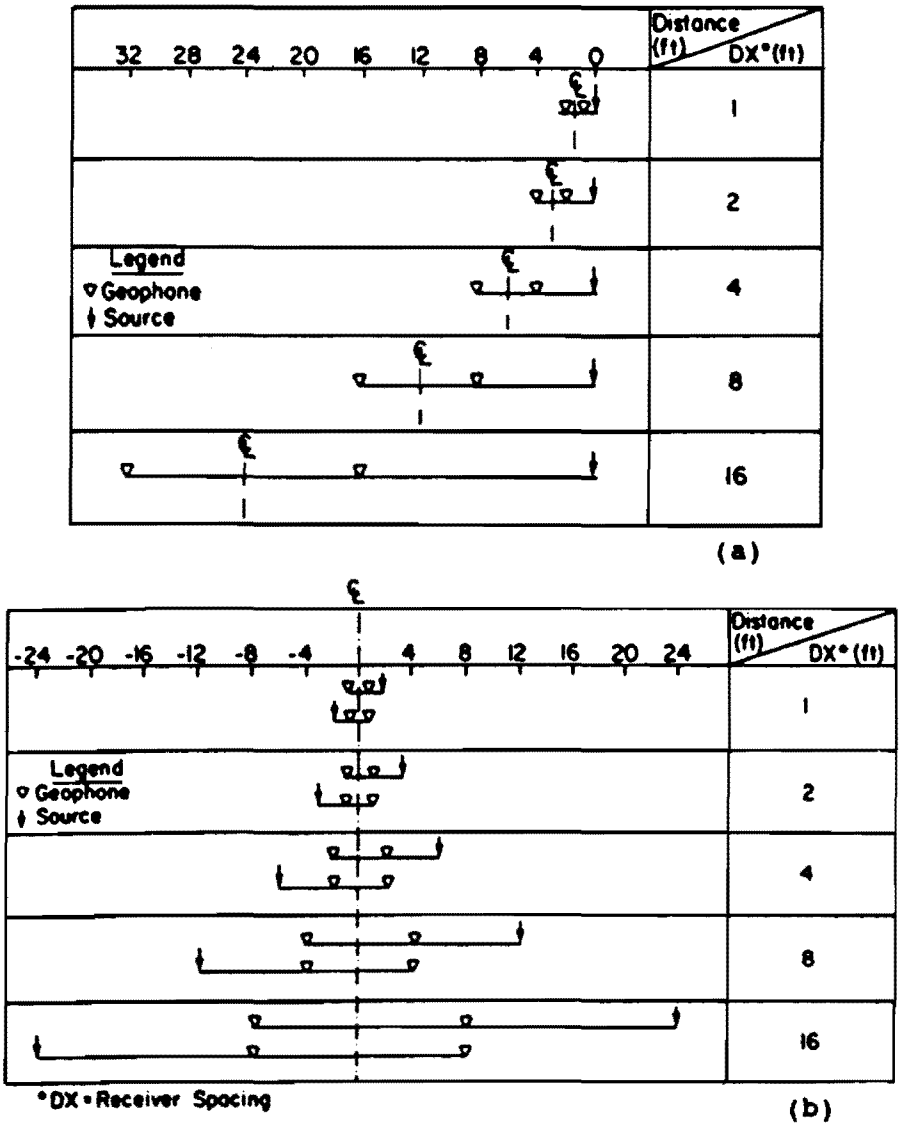

Fig. 2.2 - Common source (a) and common receiver midpoint (b) configuration

The computation of the theoretical dispersion curve of Rayleigh waves propagating in a layered medium of pavement type is essential to the backcalculation or inversion for pavement properties from the experimental dispersion data. With plane-wave approximations, this topic is discussed in Chapter 4.

The final step is the determination of the thickness and stiffness of different layers in the pavement profile from the experimental dispersion curve. This process, which is called the inversion of the dispersion curve, is described in a Chapter 5.

Chapter 3

Experimental Dispersion Curve

As indicated before, field data are in the form of phase information of cross power spectra and coherence functions from different receiver spacings.

The cross power spectrum and coherence function between records from two receivers are calculated utilizing signal processing algorithms. Let us assume that $r_1(t)$ and $r_2(t)$ are the time-domain record captured by two receivers located a distance D apart. The cross power spectrum, $\bar{S}_{r1,r2}(f)$, between these two signals is defined as (Thornhill and Smith, 1980):

$$\bar{S}_{r1,r2}(f) = \frac{1}{n}\sum_{i=n}^{n} \{ [\, R_1(f) \,]_i \cdot [\, R_2^*(f) \,]_i \} \qquad (3.1)$$

where $R_1(f)$ and $R_2(f)$ correspond the Fourier transform of $r_1(t)$ and $r_2(t)$, respectively. The bar above $\bar{S}_{r1,r2}(f)$ correspond to the frequency-domain average of several similar records. Parameter n is the number of records averaged. The asterix above $R_2(f)$ correspond to the complex conjugate operator.

Upon averaging, the coherence function, $\gamma^2(f)$, is calculated from:

$$\gamma^2(f) = \frac{|\bar{S}_{r1,r2}(f)|^2}{\bar{A}_{r1}(f) \cdot \bar{A}_{r2}(f)} \qquad (3.2)$$

where $\bar{A}_{r1}(f)$ and $\bar{A}_{r2}(f)$ correspond to the averaged auto power spectrum of records from Receiver 1 and Receiver 2, respectively. The auto power spectrum for record captured by Receiver 1, $\bar{A}_{r1}(f)$ is defined as (Thornhill and Smith, 1980):

$$\bar{A}_r(f) = \frac{1}{n}\sum_{i=1}^{n} \{ [\, R(f) \,]_i \cdot [\, R^*(f) \,]_i \} \qquad (3.3)$$

For each frequency, f, the phase shift, ϕ, is picked from the cross power spectrum. The cross power spectrum, $\bar{S}_{r1,r2}(f)$ is a complex-valued parameter. Therefore, the phase is calculated from:

$$\phi = \tan^{-1} \frac{\Im C_{r1,r2}(f)}{\Re C_{r1,r2}(f)} \qquad (3.4)$$

where the numerator and the denominator are the imaginary and real components of the cross power spectrum, respectively. Knowing the phase, the travel time (t) can be calculated by:

$$t = \frac{\phi}{360 f} \qquad (3.5)$$

and the phase velocity (V_{ph}) can be obtained by:

$$V_{ph} = \frac{D}{t} \qquad (3.6)$$

where D is the distance between the receivers. The wavelength, (L_{ph}) is related to the phase velocity and frequency by:

$$L_{ph} = \frac{V_{ph}}{f} \qquad (3.7)$$

It can be seen that if phase and frequency are known, phase velocity can be calculated using Eqs. 3.5 and 3.6.

The field data collected is contaminated with background noise. It is necessary to identify the phase data falling within the range of contaminated frequencies prior to construction of the dispersion curve. The coherence function is used for this purpose.

The coherence function has a value between zero and one in the range of frequencies being measured. A value of one indicates perfect correlation between signals being picked up by the receivers (which is equivalent to a signal-to-noise ratio of infinity). Similarly, a value of zero for the coherence function at a frequency represents no relation between the signals being detected. The phase data with low coherence value are discarded from the construction of dispersion curve.

To clarify the process, typical phase information from one cross power spectrum and associated coherence function are shown in Fig. 3.1. The receiver spacing is 600 mm. The phase plot shown in Fig. 3.1a oscillates between -180 and 180 degrees. This is the standard method of demonstrating the phase. The coherence function (Fig. 3.1b) varies between 1 and 0. Several regions with low coherence values exist in the figure. These regions are marked as shaded regions in both figures. There are several reasons for low coherence value which are discussed in Nazarian and Stokoe (1986).

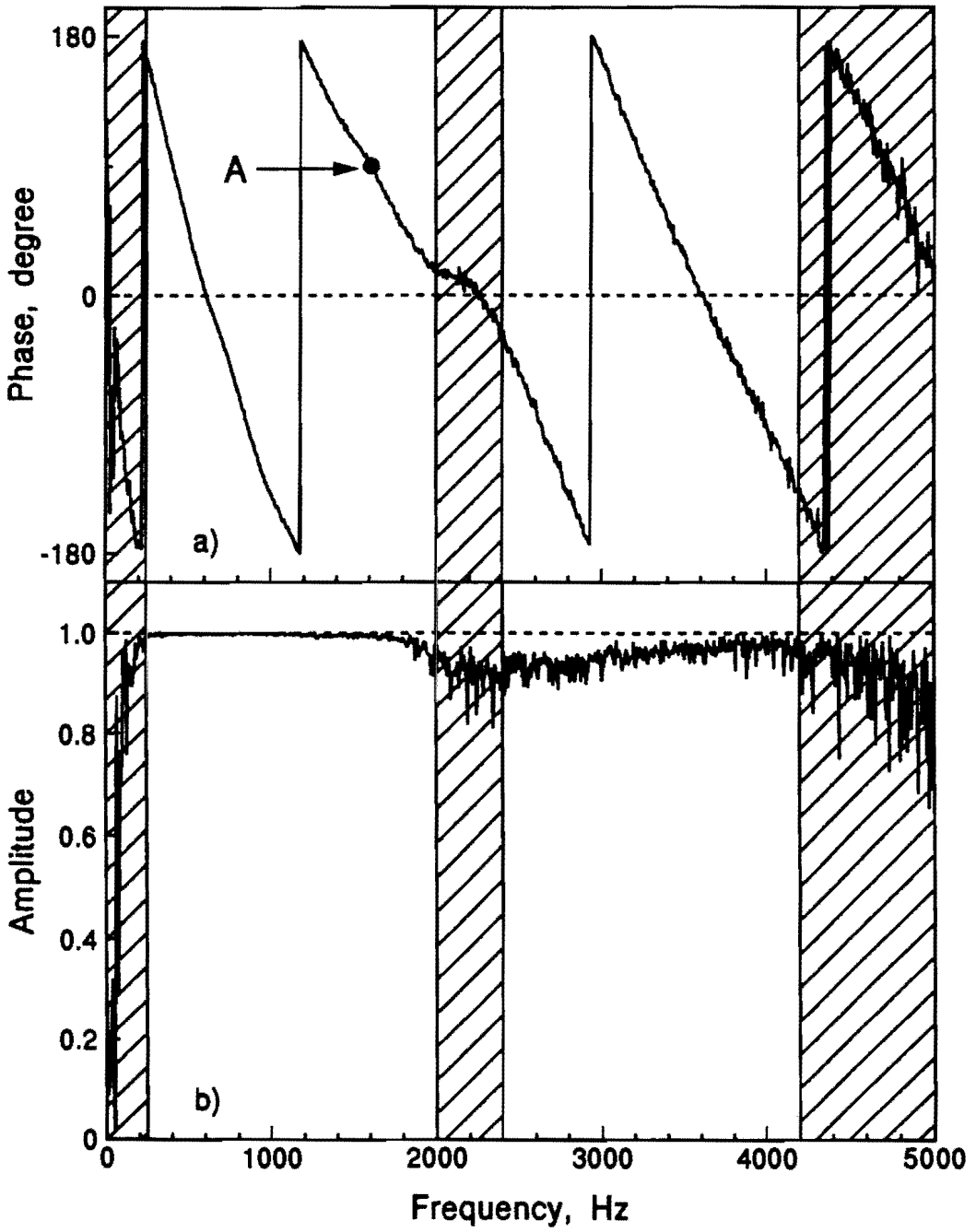

Fig. 3.1 - Typical spectral functions: a) Cross power; b) Coherence

The first step in the construction of the dispersion curve is to find the actual phase for each frequency by counting the number of 360-degree cycles preceding each frequency and adding that to the fraction of the remaining cycle to obtain the actual phase. This process is called unfolding of the phase. The phase plot in Fig. 3.1 is shown again in Fig. 3.2 after the appropriate number of cycles is added to each value of phase. As an example, one point marked as A is shown in both Figs. 3.1 and 3.2. From the raw phase data, the phase is read as 90 degrees; whereas the actual unwrapped phase is 630 degrees.

Second, the phase data falling within the low coherence ranges are discarded from the construction of dispersion curves. The low coherence ranges which are deleted are marked as shaded regions in Fig. 3.1a and Fig. 3.2.

Third, at each frequency which is not eliminated, phase velocities and wavelengths are calculated using Eqs. 3.5 through 3.7. The above procedure is repeated for all frequencies and spacings.

Fourth, the dispersion data points from records obtained at all spacings have to be combined. Usually, several thousand data points are available. These data should be combined so that a representative final dispersion curve with much less data points (several hundred) is obtained. For the use of an automated inversion routine, the number of data points can be further reduced to an order of twenty to fifty. Use of more data sampled from the same dispersion curve does not provide appreciably more independent information about subsurface structure, but the computation time may become excessively long.

Since the steps involved in identifying and eliminating the data points with a low coherence is done manually, the reduction of data is tedious and time consuming. Hence, it is necessary to develop an automated procedure for data reduction and analyses.

Automated Construction of Dispersion Curve

Theoretical Considerations

In this section, an automated procedure for construction of dispersion curve from the spectral functions (cross power spectra and coherence functions) is described. In general, two broad steps have to be taken. First, the cross power spectrum from each receiver spacing has to be mathematically defined, and, the ranges of low coherence have to be eliminated. Second, all data points from all receiver spacings have to be combined to form a representative or idealized dispersion curve. Each step is comprehensively discussed next.

Description of Cross Power Spectrum (CPS). The weighted least-squares best-fit solution (Menke, 1984) is used to describe mathematically each cross power spectrum. As indicated before, the cross power spectrum is a complex-valued function. Two nth degree polynomials are used to fit the cross power spectrum, so that the real and imaginary parts can be defined individually. Therefore, the independent variable is the frequency and the two dependent variables are the real and imaginary components of the CPS. In general terms, this problem can

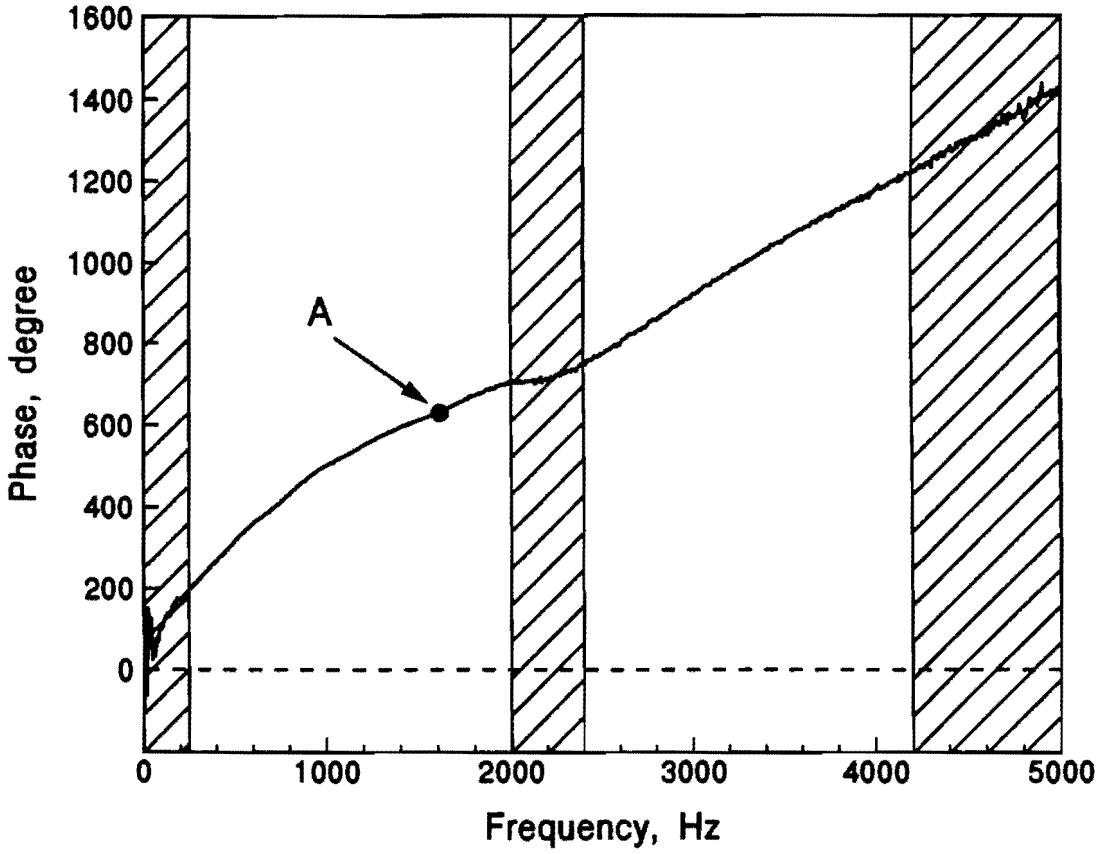

Fig. 3.2 - Unwrapped phase of cross power spectrum

be formalized as

$$G\,A = S^{obs}{}_{r1,r2} \tag{3.8}$$

where $S^{obs}{}_{r1,r2}$ is an m by 2 matrix representing the "observed" data. Parameter m is the number of data points per CPS record, and the two columns are the real and imaginary components, respectively. Matrix A is an (n+1) by 2 matrix corresponding to the coefficients of the polynomial. Once again, n is the degree of the polynomial. Matrix G, which is an m by (n+1) matrix, contains the n+1 variables used in the fitting process. In general, $G_{ij} = f_i^{(j-1)}$ where f_i corresponds to the frequency associated with the ith data point.

As the problem is overconstrained (there are more data than unknowns), the solution to the problem described in Eq. 3.8, can be written as:

$$A^{est} = [\,G^T\,G\,]^{-1}\,G^T\,S^{obs}{}_{r1,r2} \tag{3.9}$$

After the polynomial coefficients are determined, the predicted CPS values can be determined from:

$$S^{pre}{}_{r1,r2} = G\,A^{est} \tag{3.10}$$

The matrix of misfit between the observed and predicted data , e, can be defined as:

$$e = S^{obs}{}_{r1,r2} - S^{pre}{}_{r1,r2} \tag{3.11}$$

In a least-squares procedure, the goal is to minimize the square of e. Mathematically, this is is to minimize $E = e^T \,.\, e$, where E is the vector of generalized prediction error. This procedure is adequate, if the quality of the data collected is uniform. However, in our application, the effects of the data points with poor coherence should be minimized. Therefore, the generalized prediction error is redefined as:

$$E = e^T\,W_e\,e \tag{3.12}$$

where W_e is the matrix corresponding to the relative contribution of each individual error to the total prediction error.

In this study, the coherence function is used to construct the weighting matrix W_e. A threshold coherence value is selected to evaluate the quality of phase data, collected in situ. The phase data having coherence values higher than the threshold value are given more weight relative to those phase data with low coherence values.

The weighted least squares solution is then obtained from:

$$A^{est} = [G^T\,W_e\,G]^{-1}\,G^T\,W_e\,S^{obs}{}_{r1,r2} \tag{3.13}$$

Once again, the predicted data is determined from Eq. 3.10 , after the completion of simultaneous (real and imaginary components) curve fitting. In the next step, from each record,

the data points with a coherence value above the threshold are determined. For each of these data points, the phase is first determined from the real and imaginary components utilizing Eq. 3.4. The phase velocity and wavelength is then determined utilizing Eqs. 3.5 through 3.7.

Determination of Representative Dispersion Curve. For each receiver spacing, the above procedure is repeated. Dispersion data points form all receiver spacings satisfying the threshold coherence are accumulated in a data file. Typically, this yields several thousands of data points. The objective of this step is to develop a few dozens dispersion data representing the final dispersion curve.

This is done in two steps. First, the practically identical data points are eliminated to optimize the computation time. Second, a robust curve fitting scheme is utilized. These steps are described below.

Due to the experimental set up used, dispersion data points from different spacings overlap over a wide range in frequencies. Therefore, for each frequency, several dispersion data are available. A process is used to eliminate identical data points. This will reduce the number of dispersion data points from several thousands to a few hundreds. The criteria used to average data obtained at different spacings are as follows. The raw dispersion data is sorted into an ascending order with respect to wavelength, and then divided into small intervals. The intervals are chosen in a manner so that the difference between successive wavelengths within the given interval is less than three percent. The mean of wavelengths is calculated for each interval. Also for each interval, difference between successive velocities is calculated. The adjacent data points having differences less than ten percent are averaged. If the difference is greater than ten percent, then each of the adjacent points represents a single distinct data point in a given interval. In this manner, the number of data points is reduced without significantly affecting the scatter in the data. In the next step, these data points are statistically reduced to few dozen.

Up to this point, only the data with relatively low coherence or almost identical data have been eliminated from the final dispersion curve. These criteria by themselves are not adequate to remove completely all inappropriate dispersion data. The data therefore continues to be contaminated with some outliers. If these outliers are included in the estimation of the final dispersion curve, the outcome may be undesirably biased towards them. A robust curve fitting scheme, capable of minimizing the effects of these outliers is needed. It was found that a least-absolute-value best-fit or maximum likelihood estimate (L1-norm) criterion is quite appropriate for this task. An nth degree polynomial is used to fit the raw dispersion data. The independent variable is wavelength and the dependent variable is phase velocity.

In the maximum likelihood estimate, it is assumed that the statistical distribution of data is exponential. Based upon this assumption, the representative value would be the median of the data (as opposed to mean for least squares best-fit approach). The median is a robust property of a set of data (Claerabout and Muir, 1973). Adding one outlier can at worst move the median from one central datum to another nearby central datum. Therefore, least-absolute-value method is considered suitable for representing data in the presence of scatter and can efficiently handle a data set with outliers. Exponential distribution bear the same relationship to least-absolute-value as Gaussian distribution bear to least squares (Menke, 1984). The probability distribution, P(V) for m number of raw dispersion data with variance σ^2 is given as:

$$P(V) = \frac{1}{2^{\frac{m}{2}} \sigma^m} \exp\left(-2^{\frac{1}{2}} \sigma^{-1} \mid V^{obs} - V^{pre} \mid \right) \qquad (3.14)$$

where V^{obs} is a vector with m elements representing the "observed data". Parameter m is the number of raw dispersion data. Vector V^{pre} is a vector with m elements representing the "predicted" phase velocity values.

To maximize the likelihood of P(V) we must maximize the argument of the exponential, which involves minimizing the prediction error, e. Mathematically:

$$\text{Minimize } e = \mid V^{obs} - V^{pre} \mid \sigma^{-1} \qquad (3.15)$$

In least-absolute-value polynomial fitting, the goal is to determine a best approximation V^{pre} of observed phase velocity which minimizes the prediction error, e, between the observed and predicted data. The predicted phase velocity values can be represented as:

$$V^{pre} = H B \qquad (3.16)$$

where B is a vector corresponding to the n+1 coefficients of the polynomial. Matrix H, which is an m by (n+1) matrix, contains the n+1 variables used in the fitting process. In general, $H_{ij} = W_i^{(j-1)}$ where W_i corresponds to the wavelength associated with the ith data point.

The least-absolute-value problem can be converted into a linear programming problem. We introduce 2n+3m new variables d_j, c_j, j=1,n and λ_i, u_i, and v_i, i=1,m and 2n constraints. The equivalent linear programming problem is formalized as (Menke, 1984):

Minimize $\sum \lambda \sigma^{-1}$ subject to constraints

$$\sum_{i=1}^{m} \sum_{j=1}^{n} H_{ij} (d_j - c_j) + \sum_{i=1}^{m} u_i - \sum_{i=1}^{m} \lambda_i = \sum_{i=1}^{m} V_i^{obs} \qquad (3.17a)$$

$$\sum_{i=1}^{m} \sum_{j=1}^{n} H_{ij} (d_j - c_j) - \sum_{i=1}^{m} v_i + \sum_{i=1}^{m} \lambda_i = \sum_{i=1}^{m} V_i^{obs} \qquad (3.17b)$$

Provided λ_i, u_i, v_i, d_j, $c_j \geq 0$

Minimizing $\sum \lambda \sigma^{-1}$ is equivalent to minimizing the prediction error, $e = \mid V^{obs} - V^{pre} \mid \sigma^{-1}$. An algorithm developed by Barrodale and Roberts (1973) is used to solve the least-absolute-value problem. The algorithm is a modification of the standard form of the simplex method of linear programming. Using the above approach, the parameters d_j and c_j are evaluated. The polynomial coefficients, B_j are determined as follows

$$B_j = d_j - c_j \text{ for } j=1,2,.....n. \qquad (3.18)$$

After the polynomial coefficients are determined, the predicted phase velocity is determined utilizing Eq. 3.16.

The inversion process for determining the stiffness profile requires only few dispersion data points. A window averaging is carried out on the dispersion data to obtain a limited number (20 to 50) of idealized dispersion data.

The dispersion data is first divided into three equal data sets with respect to wavelength. Fifty percent of idealized dispersion data are selected from the first set. The second set contains thirty eight percent of idealized dispersion data, and the third set contains twelve percent of idealized dispersion data. Based on much experience, these values are suitable for most sites.

The division of the dispersion data into three equal data sets with respect to wavelength helps in retaining the various features of the dispersion curve. At short wavelengths, sub-surface exhibits large variations in phase velocity, therefore it is necessary that the first set contain relatively more number of idealized data points than the other sets.

For each set, a small wavelength window is selected, the height of the window (ΔW) is given as

$$\Delta W_i = (WMAX_i - WMIN_i) / N_i \quad \text{for } i = 1 \text{ to } 3 \tag{3.19}$$

where $WMIN_i$ is the minimum wavelength and $WMAX_i$ is the maximum wavelength pertaining to a given set. Parameter $WMIN_1$ is set as the minimum wavelength measured in sites and $WMAX_3$ is equal to the maximum wavelength measured in sites. A moving window averaging process is employed to determine each data point. The height of the window is equal to ΔW_i determined from Eq. 3.19. The representative wavelength for a given window is assumed as the midheight of the window. The representative phase velocity is simply determined by calculating the arithmetic mean of all data points in the window.

Practical Considerations

To clarify the process, typical phase information from one cross power spectrum and the associated coherence function shown in Fig. 3.1 are used.

The first step is to find the weighted least squares best-fit solution of cross power spectrum. The real and imaginary components of the cross power spectrum are divided into eight sets of equal points. In addition, ten extra points are used for overlap. The real and imaginary components of the cross power spectrum shown in Fig. 3.1 are shown in Fig. 3.3 along with the eight regions used. The division of the cross power spectrum into eight sets was chosen for the following reasons. First, with fewer number of data points a lower degree polynomial can be effectively used to determine the best-fit curves. Second, curve fitting with a low degree polynomial requires less computer memory and computation time.

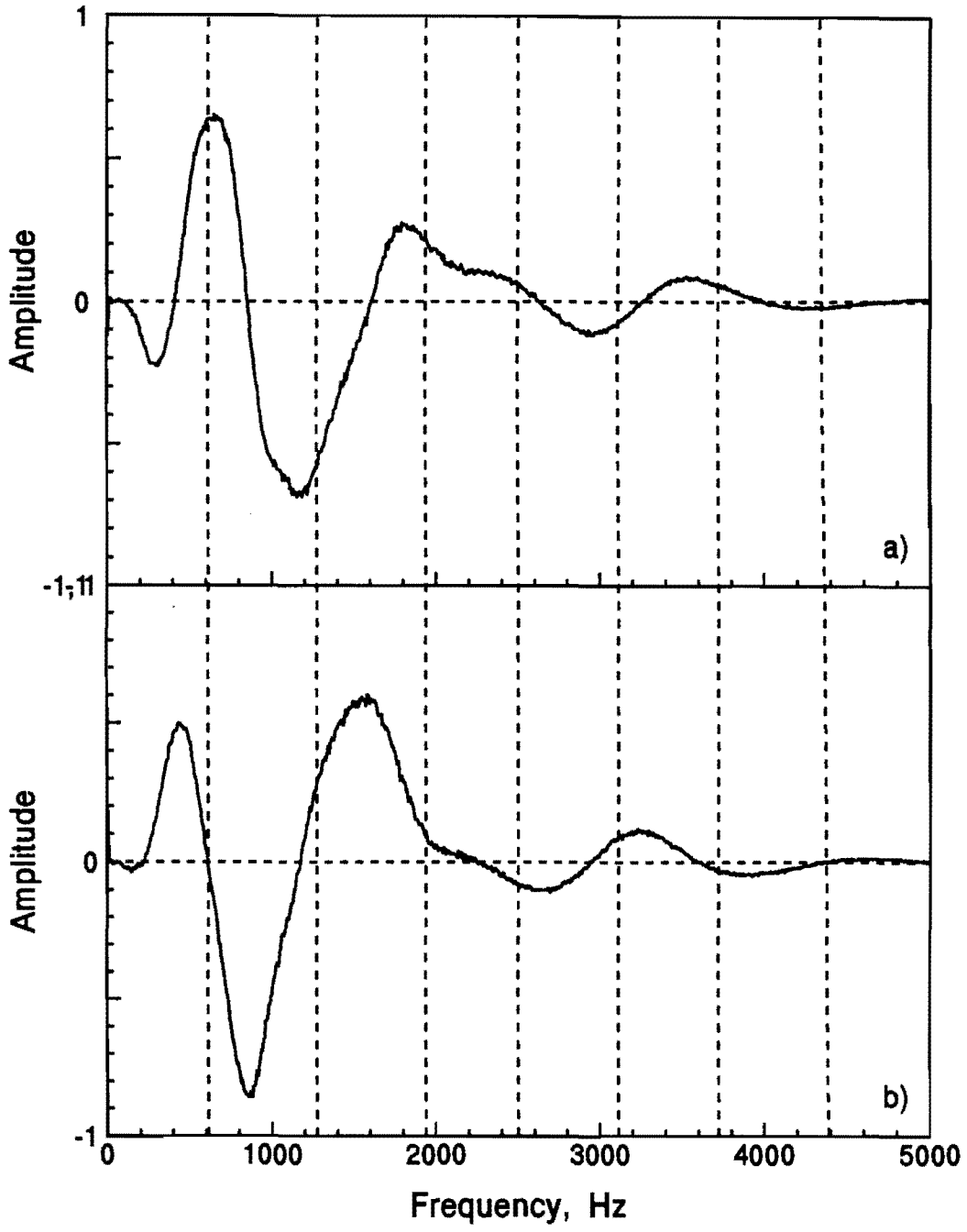

Fig. 3.3 - Real a) and imaginary b) components of cross power spectrum

Different combinations of numbers of data points and degrees of polynomial were examined over many different field data. The coefficient of variation was used to judge the quality of the fit. It was found that, in almost all cases, each set of data from the eight-region division fitted with a second degree polynomial yielded the most computationally efficient results with a minimal sacrifice in the quality of data.

Each data set has an overlap of ten data points with the neighboring data sets. These data points are used for smoothing the transition between the two adjacent data sets. After the curve fitting, the first and last five data points from each data set are ignored. In this manner, the transition is carried out quite smoothly.

The coherence function is used to construct the weighing matrix W_c. Based upon the experience of Nazarian and Stokoe (1986), a threshold value of 0.9 is selected to evaluate the quality of phase data collected in situ. In the curve fitting process, phase data having coherence values higher than the threshold value are given weights that are twice of those phase data with low coherence values. The predicted values of the real and imaginary components of the cross power spectrum are shown in Fig. 3.3. The vertical dotted lines in Fig. 3.3 show the eight divisions of the cross power spectrum utilized in the curve fitting process. The curves obtained from both methods compare well. Variations between the two curves are seen between frequencies 0 to 250 Hz, 2000 to 2400 Hz, and 4200 to 5000 Hz. The variations are in the ranges where the data have low coherence values. These ranges are marked as shaded regions in Fig. 3.3.

The phase from the weighted least-squares best-fit solution is shown in Fig. 3.4. The vertical dotted lines in Fig. 3.4 show the eight divisions of the cross power spectrum utilized in the curve fitting process. Some disagreement between the observed and the predicted phases can be seen in the ranges where the quality of phase data is poor. These ranges, marked as shaded regions in Fig. 3.4, are discarded from calculations.

In the second step, the phase data with coherence values above the threshold coherence are determined. The data points having a phase of less than 120 degrees are eliminated from calculations, as recommended by Nazarian and Stokoe (1986) and Sheu et al. (1987). Therefore, only the phase data greater than 120 degrees having coherence values above 0.9 are selected to obtain the phase velocity and wavelength (utilizing Eqs. 3.5 through 3.7).

The raw dispersion data obtained from the original method and the automated method are compared in Fig. 3.5 for the one record shown in Fig. 3.1. The gaps seen in the dispersion data correspond to data points with low coherence values. The two curves compare quite well, indicating the appropriateness of the curve fitting process. The above procedure is repeated for all frequencies and spacings.

The almost identical dispersion data points from records obtained at all spacings are then eliminated. As indicated, an averaging process is utilized to reduce the number of dispersion points from several thousands to a few hundreds. The criteria used for the averaging process is described in the preceding section. The raw dispersion data points obtained after eliminating almost identical data for all spacings are shown in Fig. 3.6. The raw dispersion data are

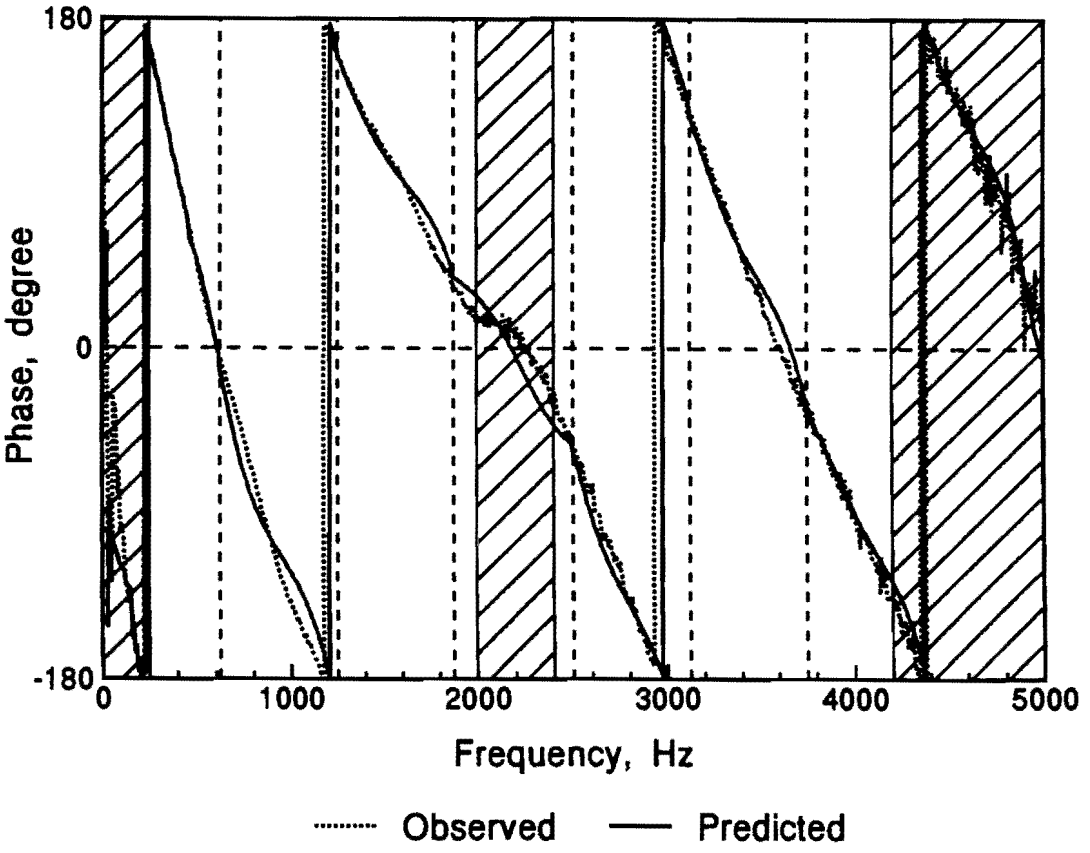

Fig. 3.4 - Comparison of observed and predicted cross power spectra

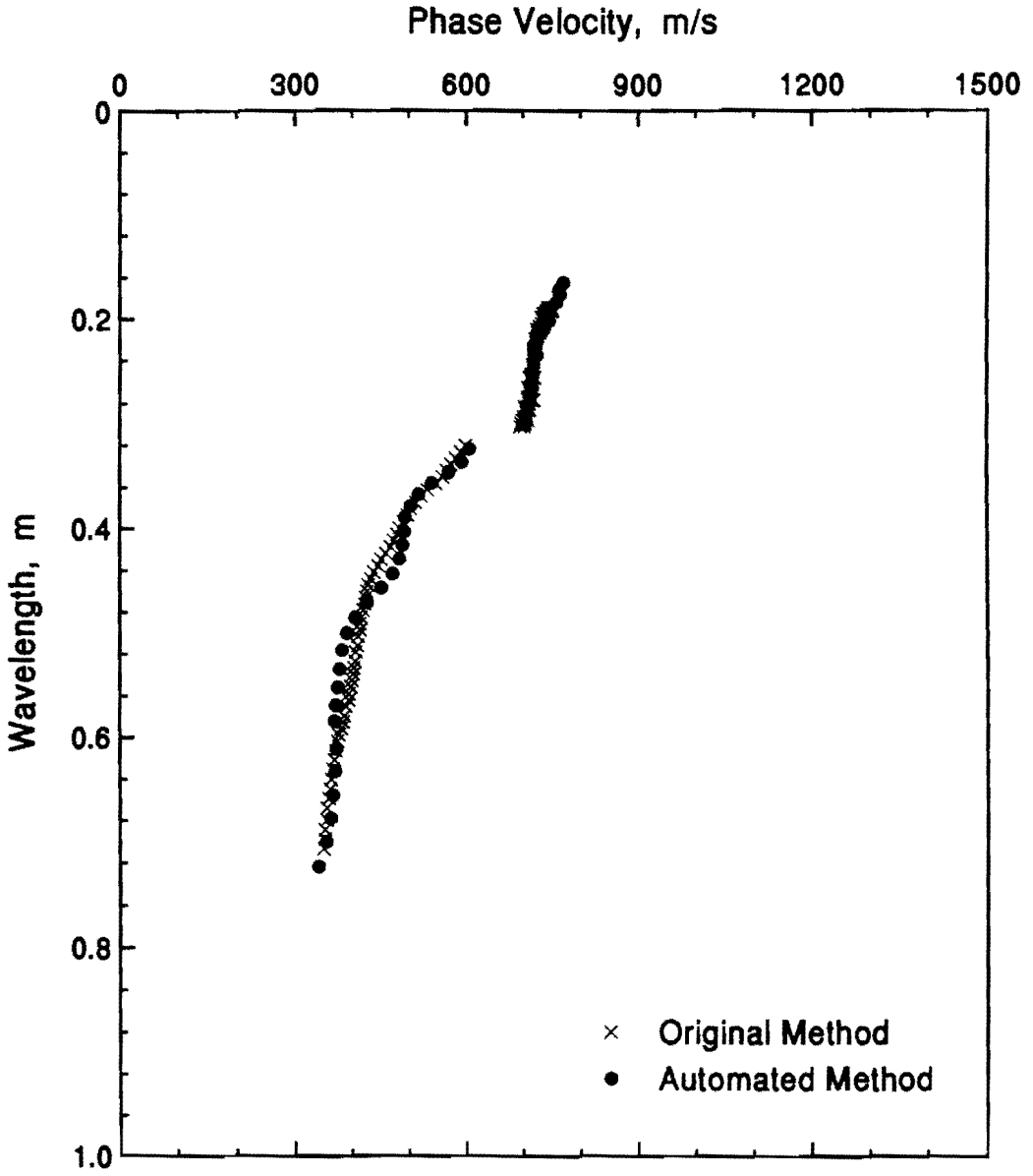

Fig. 3.5 - Comparison of raw dispersion data obtained from two methods

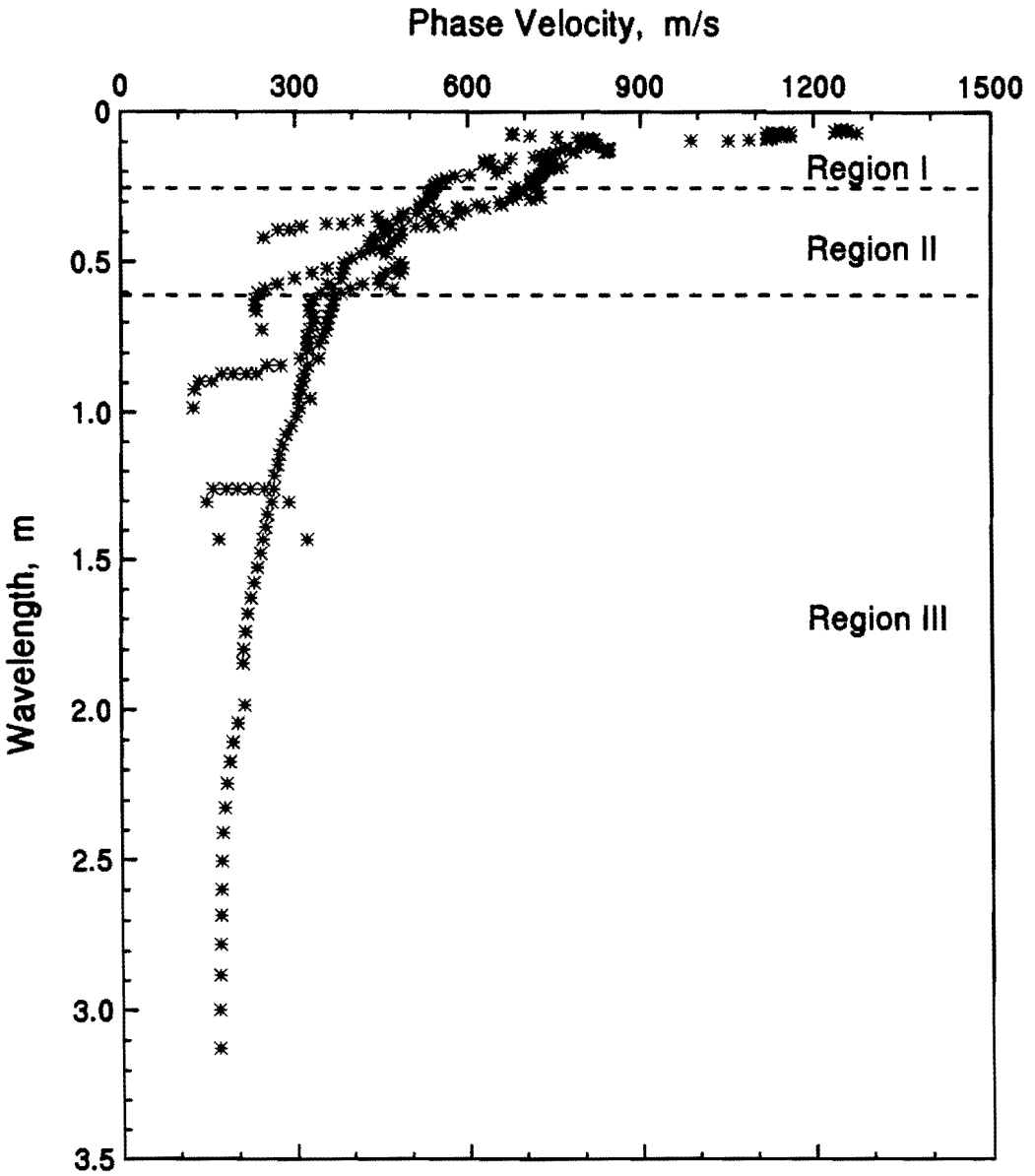

Fig. 3.6 - Raw dispersion data obtained from all receiver spacings

contaminated by quite a few outliers. This indicates that the coherence criteria by itself may not be adequate to eliminate all undesirable data.

The raw dispersion data are then combined using the least-absolute-value best-fit criterion to construct an idealized dispersion curve. The raw dispersion data is divided into 3 equal sets, as shown in Fig. 3.6. Each set is provided with 20 extra points. These extra data points are used for smoothing purposes. The procedure utilized is similar to those used for smoothing cross power spectra.

The division of the dispersion data into three sets is quite important. In this manner, the basic features of the dispersion curve are preserved. Significant number of data points are concentrated in shallow wavelengths. Even though, desirable for pavement sites, this may not be optimal for soil sites.

A fourth degree polynomial is used to fit each set of raw dispersion data. The least-absolute-value best-fit solution obtained for each of three data sets is then combined to form the final dispersion curve.

The least-absolute value best-fit solution for the raw dispersion curve is shown in Fig. 3.7. The dispersion curve obtained for all spacings using original method is also included in Fig. 3.7. It is seen that the curves obtained from both methods compare well. A slight difference of less than three percent is seen at longer wavelengths. This can be attributed to the fact that few dispersion data points are available at longer wavelengths, and therefore the accuracies of both systems are slightly reduced.

In the last step, a window averaging process is carried out on the dispersion data to obtain a few dozen idealized data points to be used for an automated inversion process. The dispersion data is divided into three sets with respect to wavelength. The minimum and maximum wavelengths are measured at the site. Fifty percent of fifty idealized dispersion data are assigned to the first set which corresponds the shorter wavelengths. The second set contains thirty-eight percent of fifty idealized dispersion data, and the third set which corresponds the longer wavelengths contains twelve percent of fifty idealized dispersion data.

The dispersion data points falling within the window are averaged. A plot of the idealized dispersion curve for all spacings at the site is shown in Fig. 3.8. The horizontal dotted lines in Fig. 3.8 show the three regions of the dispersion curve utilized in the window averaging process.

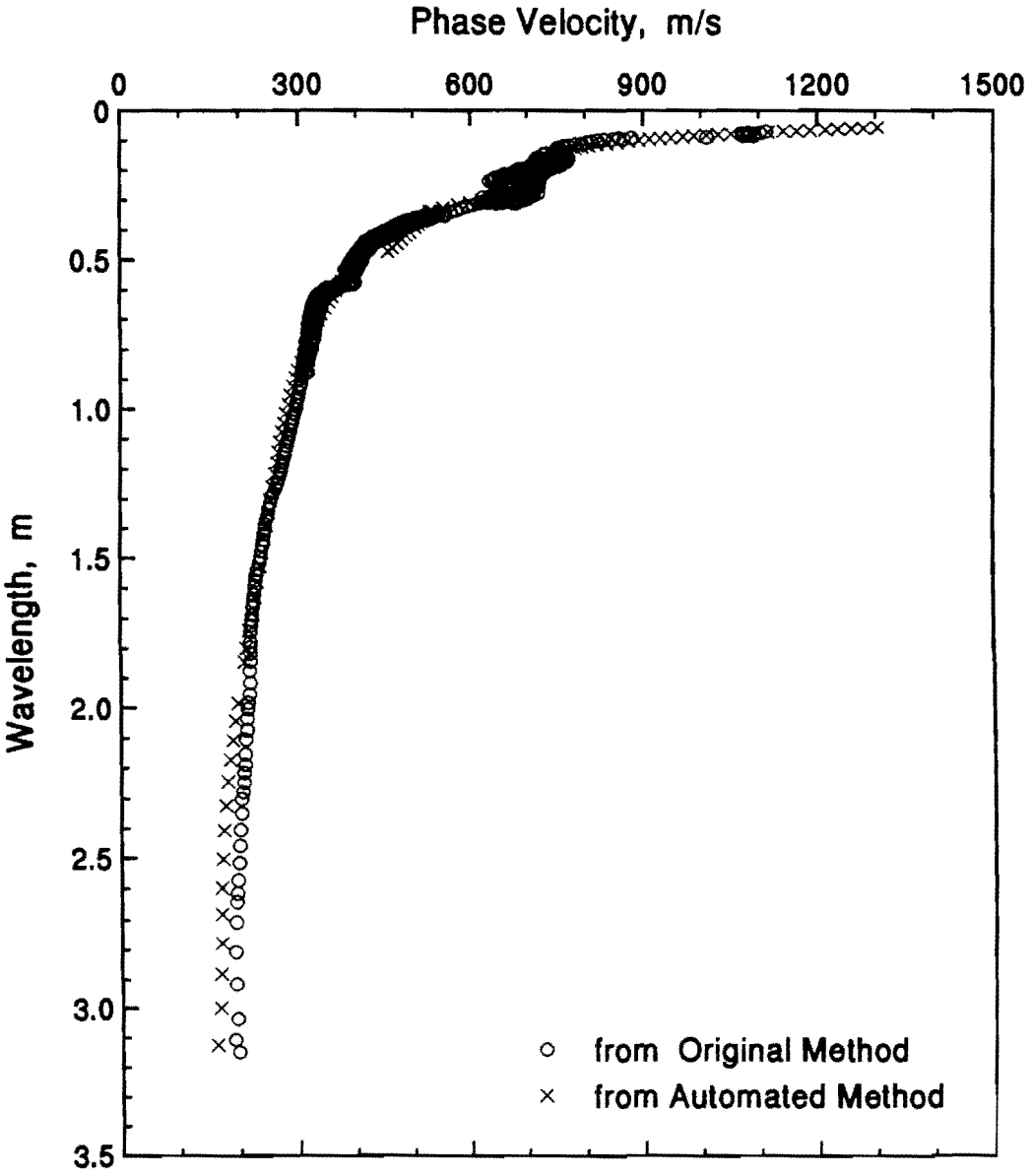

Fig. 3.7 - Comparison of dispersion curves obtained from two methods

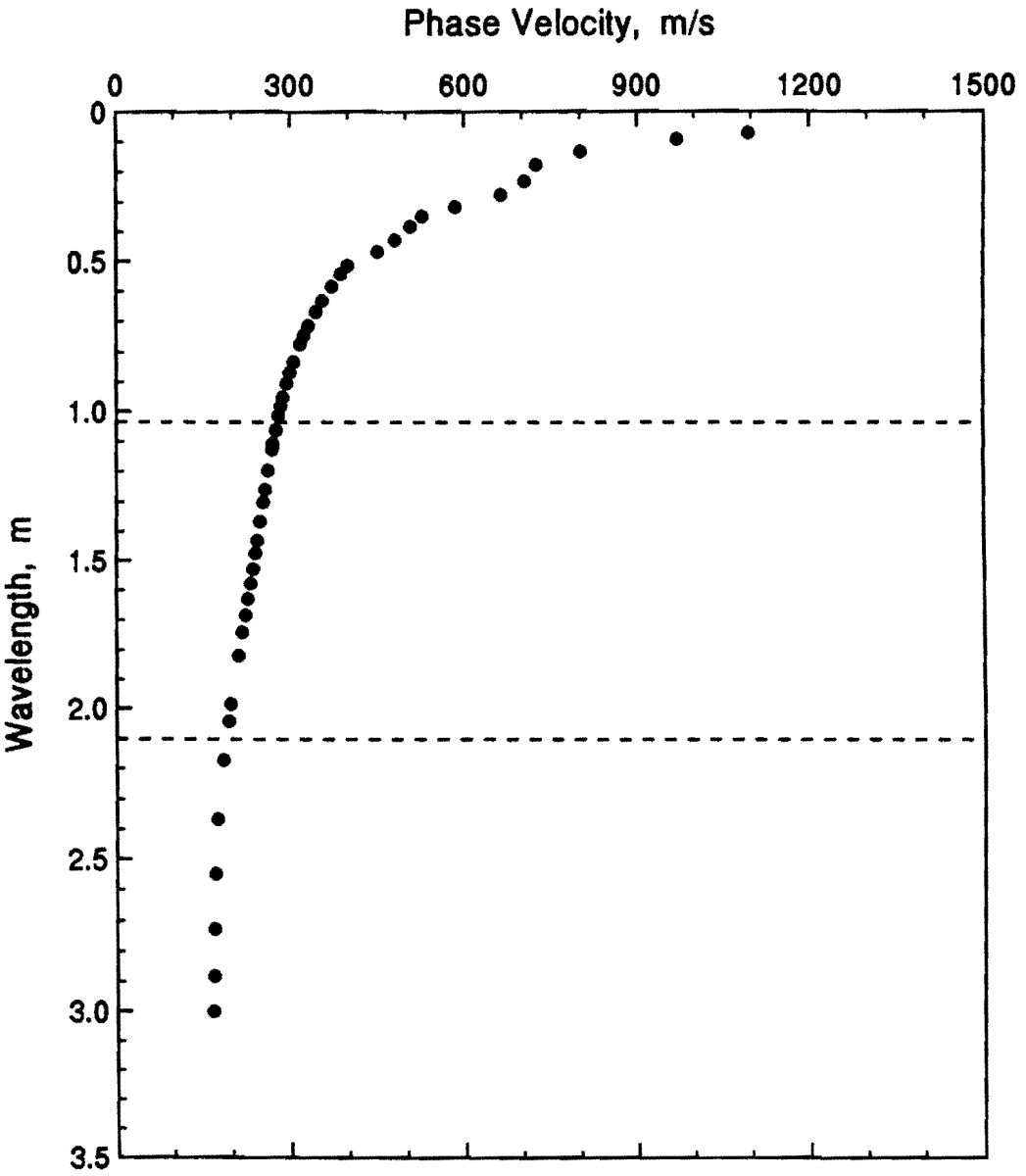

Fig. 3.8 - Idealized dispersion curve obtained from all receiver spacings

Chapter 4

Theoretical Dispersion Curve

Any technique for determining the shear wave velocity profile of a site from an experimental dispersion curve involves a procedure that minimizes the difference between the experimental dispersion curve and theoretical one calculated from a trial profile. Thus, the calculation of theoretical dispersion curve is an important task in the SASW method. This task may become more important for pavements because the stiffness decreases with depth.

Basic Assumptions

Shown in Fig. 4.1 is an idealized cross section of a pavement. To apply the theory of wave propagation to this profile, two major assumptions are made. First, it is assumed that only the in-plane waves are involved so that problem can be approximated as a plane strain problem. Second, it is assumed that the system is composed of a stack of flat layers with homogeneous and isotropic properties, and each layer extends horizontally to infinity (as compared with the dimension of source-receiver configuration). The effects of these two assumptions either are minor (Sanchez et al., 1987) or can be minimized with proper setup in field testing (Sheu et al., 1987). With these assumptions, the solution to the wave equation reduces to a simple two-dimensional problem in the Cartesian coordinate system.

The parameters needed to define the properties of each layer are thickness (h), shear wave (S-wave) velocity (V_s), compressional wave (P-wave) velocity (V_p) or Poisson's ratio (ν), and mass density (ρ). Amongst these parameters, S-wave velocity has the dominant effect on surface wave dispersion, and the effects of mass density and Poisson's ratio are rather small. Nazarian (1984) has numerically shown that the effects of these two parameters, in most practical cases, are less than five percent. Therefore, to simplify the inversion process, one can assume that density and Poisson's ratio of each layer are known. Reasonable values can be assigned to these parameters based upon experience. Shear wave velocity of each layer is the only active parameter to be determined.

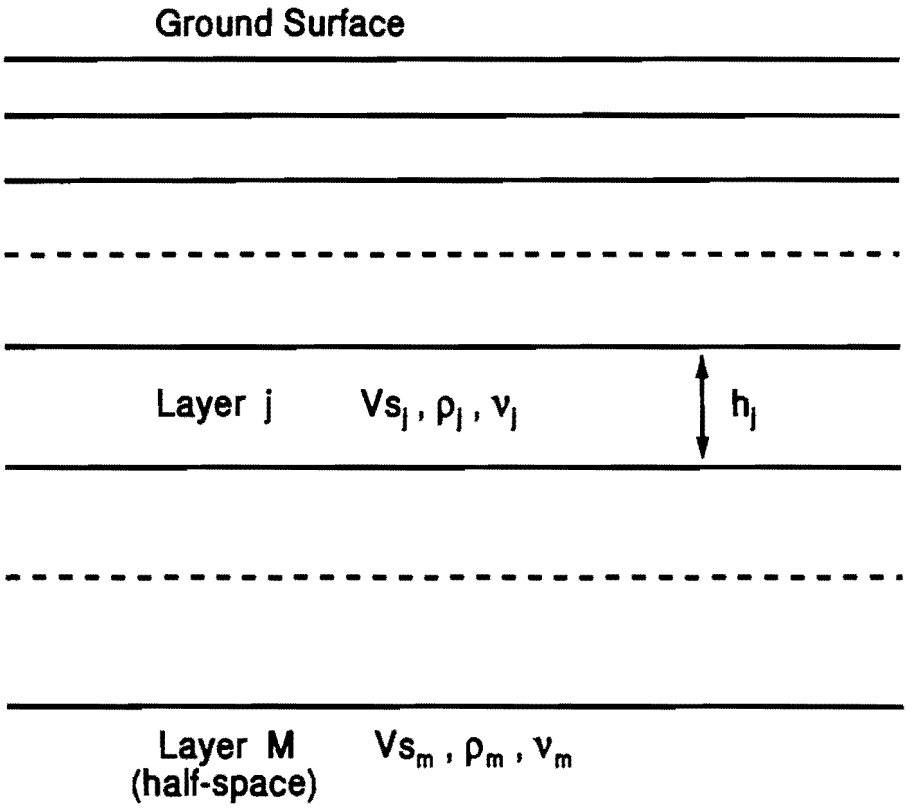

Fig. 4.1 - Idealized profile of a pavement system

Basic Formulation

With the plane-wave approximations, two similar approaches — the transfer matrix approach (Haskell, 1953) and the stiffness matrix approach (Kausel and Roesset, 1981) — are currently adopted in the SASW method to calculate a theoretical dispersion curve. The two approaches may ultimately lead to solving a secular equation of the same form. In this study, dispersion calculations were carried out through the transfer matrix approach with real wavenumber analysis and necessary treatments for mode isolation and root refining.

The theoretical dispersion curve is obtained by determining the Rayleigh wave phase velocity at different frequencies (wavelengths) using the theory of plane wave propagation in layered media. This has been a well-studied topic since the transfer matrix method was introduced. Here only an outline of the method is presented.

It is convenient to start the problem with displacements and stresses because they are the quantities used in imposing boundary conditions and are needed to solve the problem. The equations of motion for Rayleigh or P-SV type waves (in the x-z plane) in terms of displacements at any point in an elastic layered system are

$$\rho \frac{\partial^2 u}{\partial t^2} = (\lambda + 2G) \frac{\partial^2 u}{\partial x^2} + (\lambda + G) \frac{\partial^2 w}{\partial x \partial z} + G \frac{\partial^2 u}{\partial z^2} \qquad (4.1)$$

$$\rho \frac{\partial^2 w}{\partial t^2} = (\lambda + 2G) \frac{\partial^2 w}{\partial z^2} + (\lambda + G) \frac{\partial^2 u}{\partial x \partial z} + G \frac{\partial^2 w}{\partial x^2} \qquad (4.2)$$

where u = horizontal displacement, w = vertical displacement, t = time, G = shear modulus, λ = Lame's constant, and ρ = mass density.

Equations 4.1 and 4.2 have general solutions of the following form

$$u = r_1(z;\omega,k) \exp[i(kx - \omega t)] \qquad (4.3)$$

$$w = i r_2(z;\omega,k) \exp[i(kx - \omega t)] \qquad (4.4)$$

where $i = \sqrt{-1}$, $\omega = 2\pi f$ is angular frequency, and k is wavenumber.

Correspondingly, the shear and normal stresses on a horizontal plane which are continuous in the z-direction are given by

$$\sigma_{zx} = r_3(z;\omega,k)\exp[i(kx - \omega t)] \tag{4.5}$$

$$\tau_{zz} = ir_4(z;\omega,k)\exp[i(kx - \omega t)] \tag{4.6}$$

For simplicity of notation, vector s is introduce so that

$$s = (u,\ w,\ \sigma,\ \tau)^T \tag{4.7}$$

At the interface of any two layers in a layered system, the continuity of displacements and stresses requires that:

$$s_{j+1}^{<T>} = s_j^{<B>} \tag{4.8}$$

where superscripts <T> and <B> denote the top and bottom of a layer, respectively. For any layer, the displacements and stresses at the top of the layer can be related to the displacements and stresses at the bottom of the same layer (the top of the underlying layer) through a 4x4 matrix. This relationship can be written as

$$s_j^{<B>} = T_j s_j^{<T>} \tag{4.9}$$

Substituting Eq. 4.8 into Eq. 4.9 results in

$$s_{j+1}^{<T>} = T_j s_j^{<T>} \tag{4.10}$$

By applying the process to all layers, a relationship between the displacements and stresses at the ground surface and at the top of the half-space (or at any interface) in a layered system of M layers can be obtained through matrix multiplication

$$s_M^{<T>} = T_{M-1}T_{M-2}\cdots T_1 s_1^{<T>} \tag{4.11}$$

Matrix T is called the transfer matrix. The expression for this matrix can be found in a number of publications. The reader is referred to the representative works of Haskell (1953) for the original formulation, and Dunkin (1965) and Watson (1970) for solutions which minimize the problem with loosing numerical precision at high frequencies.

Introducing a new matrix

$$R = \prod_{j=1}^{M-1} T_j = \begin{bmatrix} r_{11} & r_{12} & r_{13} & r_{14} \\ r_{21} & r_{22} & r_{23} & r_{24} \\ r_{31} & r_{32} & r_{33} & r_{34} \\ r_{41} & r_{42} & r_{43} & r_{44} \end{bmatrix} \tag{4.12}$$

and considering the boundary condition at the ground surface and the radiation condition for the homogeneous half-space (or layer M) where waves can only travel downwards, we have

$$\begin{bmatrix} 0 \\ 0 \\ -- \\ P_d \\ S_d \end{bmatrix} = \left[\begin{array}{cc:cc} r_{11} & r_{12} & r_{13} & r_{14} \\ r_{21} & r_{22} & r_{23} & r_{24} \\ \hdashline -- & -- & -- & -- \\ r_{31} & r_{32} & r_{33} & r_{34} \\ r_{41} & r_{42} & r_{43} & r_{44} \end{array}\right] \begin{bmatrix} u_1 \\ w_1 \\ -- \\ 0 \\ 0 \end{bmatrix} \qquad (4.13)$$

where P_d and S_d indicate the components of waves traveling downwards in the half-space which make no contribution to surface waves. Equation 4.13 has a non-trivial solution if, and only if

$$\Delta(\omega,k) = \det\begin{bmatrix} r_{11} & r_{12} \\ r_{21} & r_{22} \end{bmatrix} = 0 \qquad (4.14)$$

This equation, which is known as the period or secular equation of Rayleigh waves, relates frequency to wavenumber or phase velocity. It represents an eigenvalue problem; that is, for a given frequency, non-trivial solutions (displacements, u and w, or eigenfunctions) exist only for certain wavenumbers (eigenvalues). Then the phase velocity is given by $c = \omega/k(\omega)$, and the corresponding wavelength $L = c/\omega$.

The root of Eq. 4.14 is determined by fixing ω and varying c (from an underestimated initial value) until the determinant has sign change. This includes two tasks: bracketing the root at a given frequency for the desired mode (it is the fundamental mode in the SASW method) and refining it until a specified accuracy is achieved.

As stated earlier, the dispersion modes of Rayleigh waves in a pavement system are mathematically analogous to the so-called leaky modes. For leaky modes, the solution to the secular equation is possible when at least one of the three parameters involved (i.e. frequency, wave number, or phase velocity) are complex (Alsop, 1970). For a given profile, different approaches may lead to slightly different theoretical dispersion curves. From a "physically" intuitive viewpoint, the dispersion curve for real frequency would be preferred.

A critical frequency exists when the propagation of Rayleigh waves in a pavement system is studied. At frequencies higher than this frequency, Eq. 4.14 becomes complex and there are no real solutions for the phase velocity that satisfies both real and imaginary parts of $\Delta(\omega,k)$. To obtain a dispersion curve that may extend over the entire frequency range, only the real part of $\Delta(\omega,k)$ is considered to obtain a solution to Eq. 4.14.

The dispersion curves obtained from the formulation and treatments described above have been compared with those obtained from an axisymmetric analysis with complex wavenumber made by Vidale (1964). Results from the two different approaches are quite consistent. As an example, Fig. 4.2 shows the dispersion curves for a simple profile of a stiff layer over a softer half-space. All features of the two curves are similar with only slight differences in phase velocities.

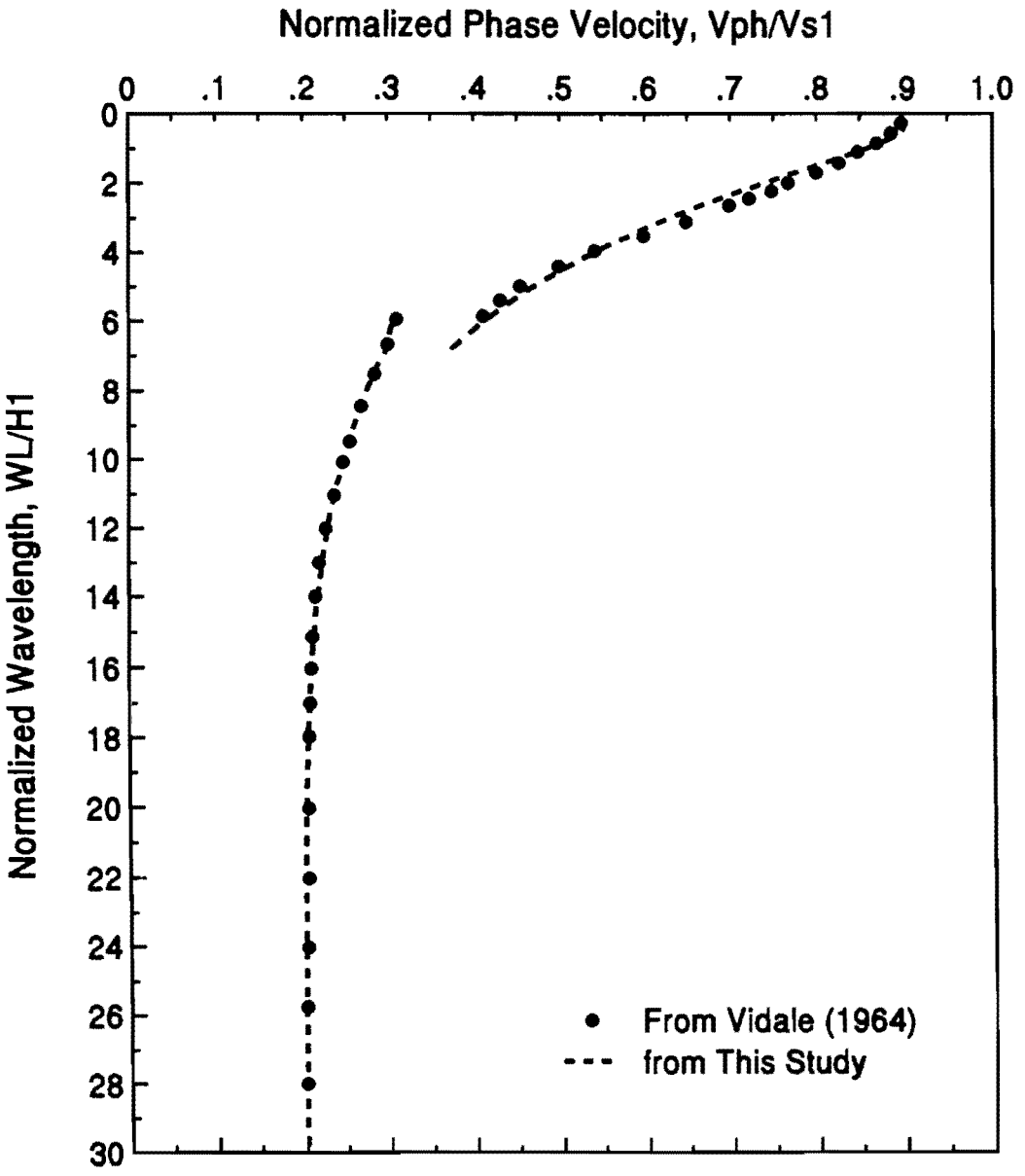

Fig. 4.2 - Comparison of theoretical dispersion curves obtained from two different approaches for a two-layer profile

Dispersion Characteristic

The general characteristic of the abnormal dispersion can be demonstrated by the dispersion curve shown in Fig. 4.3. The curve corresponds to a three-layer system of two stiff layers over a softer half-space. In the figure, phase velocities have been normalized with respect to the shear wave velocity of the top layer, and wavelengths have been normalized with respect to the thickness of the top layer.

Although not shown here, phase velocity is equal to the Rayleigh wave velocity of the half-space at very low frequencies and increases continuously as frequency increases (wavelength decreases) until the shear wave velocity of the half-space is reached at a critical frequency. This frequency depends on the thicknesses and the velocity contrasts of layers. As indicated before, for frequencies higher than this frequency, Eq. 4.14 becomes complex, and there are no real solutions for the phase velocity that may satisfy both real and imaginary parts of the determinant in the equation. To obtain phase velocities at higher frequencies (shorter wavelengths), only the real part of the determinant is considered.

The dispersion curve for a pavement system consists of branches and the number of branches in most cases is equal to the number of distinct layers in the system. Physically, these branches are caused by the geometric attenuation (in addition to the annular divergence) and the downward radiation (leakage) of vibration energy (Ewing et al., 1957; Jones, 1962).

The characteristic of each branch is related to the thickness and body wave velocities of the corresponding layer. The branch for the half-space approaches the Rayleigh wave velocity and P-wave velocity of the half-space at very long and short wavelengths, respectively. The branch associated with the top layer approaches the P-wave velocity and Rayleigh wave velocity of that layer at long and short wavelengths, respectively.

For other layers in the profile, the upper and lower bounds of the branch are determined by the P- and S-wave velocities of those layers (see Fig. 4.3). At short wavelengths, the branch approaches the P-wave velocity of the layer. The rate at which the phase velocity approaches the P-wave velocity depends on the Poisson's ratio of the layer (see Fig. 4.4). Also, each branch may have a high-frequency cut-off (short wavelength limit), depending on the Poisson's ratio. Waves corresponding to the branches other than first one can only exist at wavelengths greater than the short wavelength limit (see Fig. 4.4).

It should be pointed out that although different approaches may result in slightly different theoretical dispersion curves for a pavement profile, the branch feature of dispersion is basically independent of the solution approaches being used. For example, approaches that involve complex "phase velocity" (Jones, 1962), complex wave number (Vidale, 1964), and complex frequency (Nazarian, 1984), respectively, all lead to the branched dispersion curves.

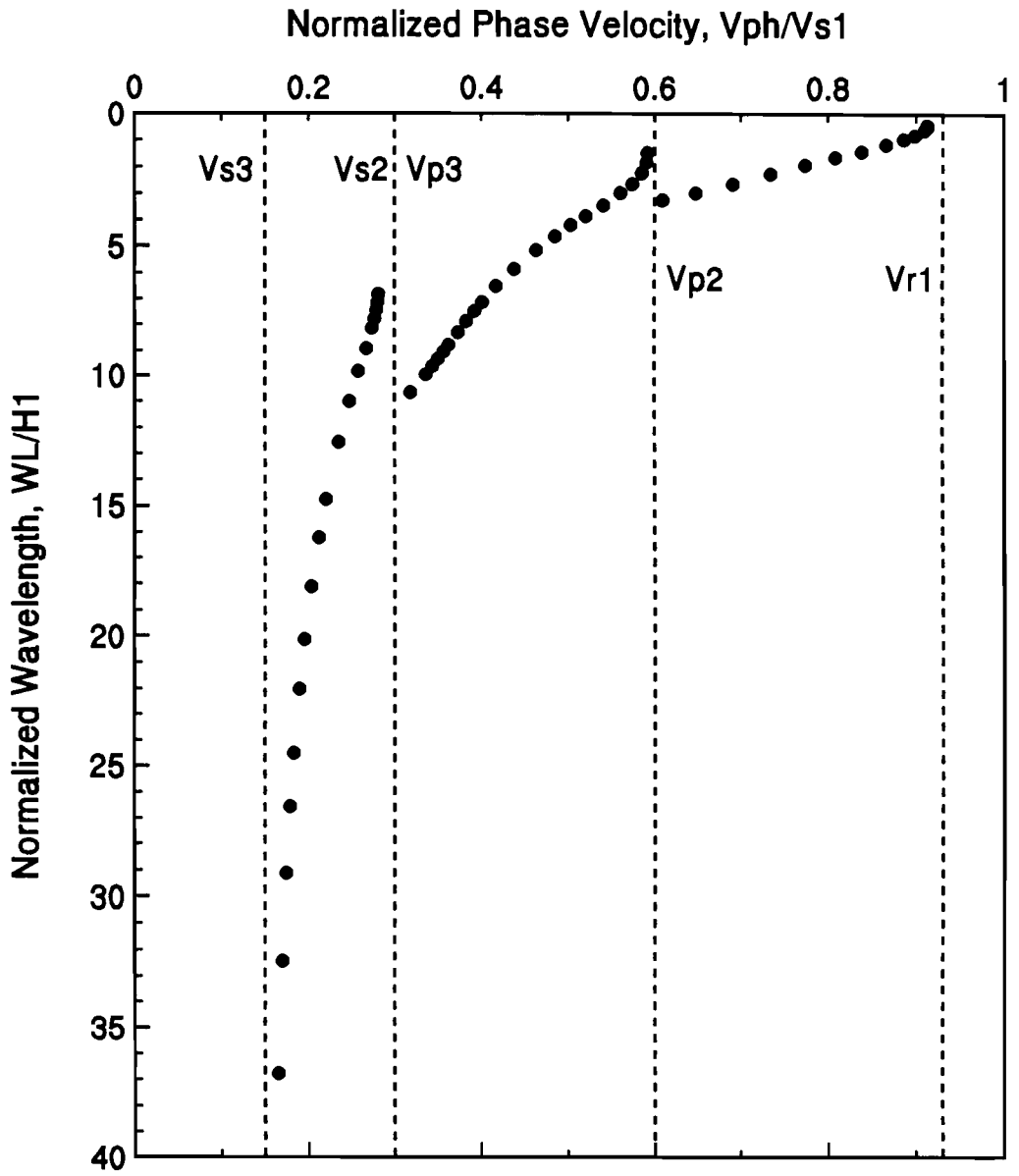

Fig. 4.3 - Dispersion curves for a three-layer profile

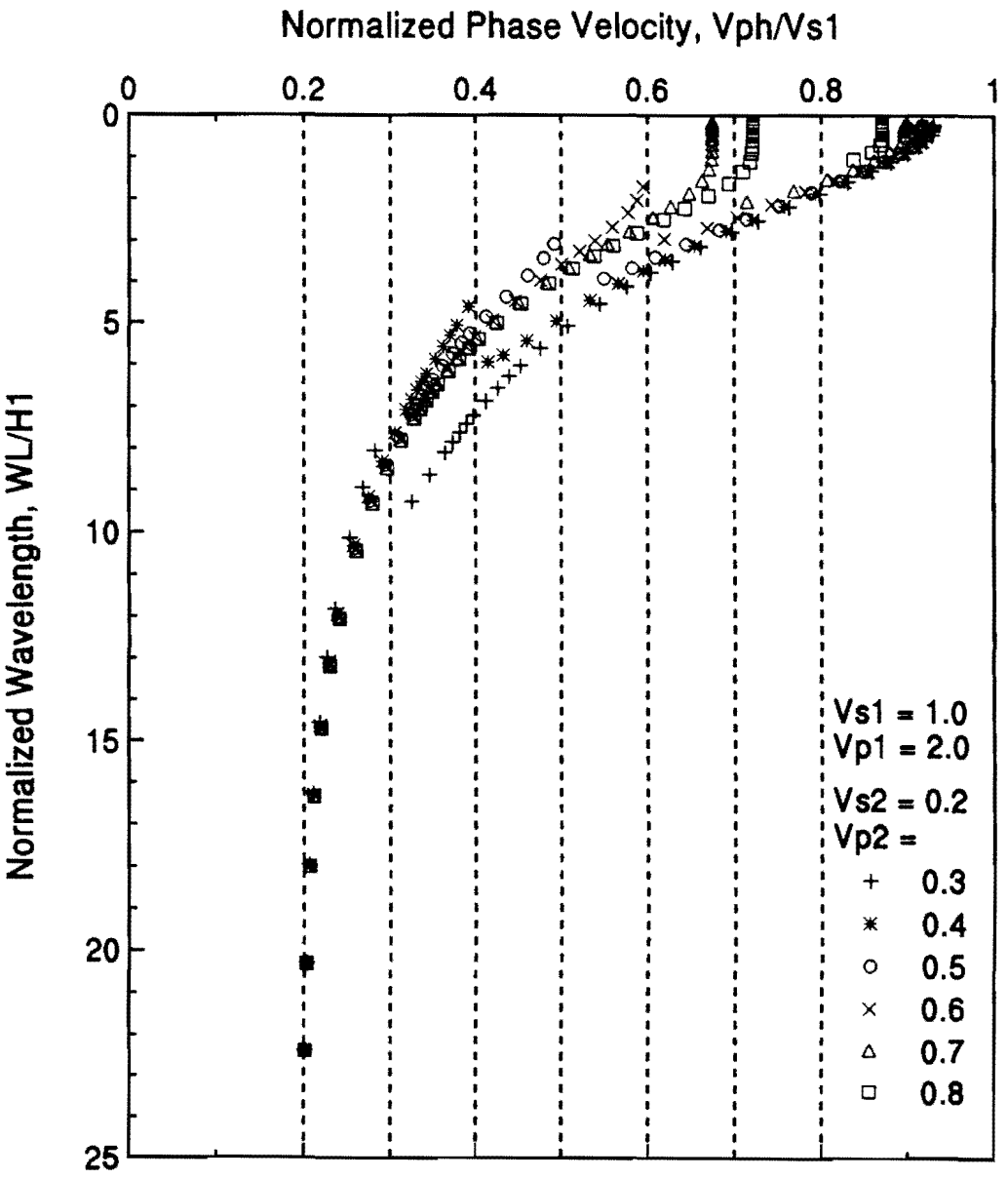

Fig. 4.4 - Effect of P-wave velocity on branches

Chapter 5

Inversion Process

An inversion algorithm has been developed and is described in this chapter. The algorithm, which is based upon the general inverse theory (Jackson, 1972), provides an automatic iterative procedure for rapidly determining shear wave velocity or modulus profiles from dispersion curves. At the same time, the algorithm yields information needed for uncertainty analysis of the results obtained from the inversion process.

Layer thicknesses can be estimated in two ways. They can either be assumed as known or can be determined through the inversion process (Yuan and Nazarian, 1993). If layer thicknesses are assumed as known parameters, it is necessary to include a number of (about 10) thin layers with fixed thicknesses in the trial profile to minimize the biased effects of interfaces on resulting profile. This is necessary because the interpretation of layer thickness is done by determining layer interfaces with significant velocity or modulus contrast. If both thicknesses and shear wave velocities need to be simultaneously determined, only a few (3 to 6) layers will be required.

To simplify the inversion process, one can assume that density and Poisson's ratio for each layer are known parameters. Reasonable values can be assigned to these parameters based upon experience and other information. Shear wave velocity of each layer is the only active physical parameter to be determined.

Assume that the SASW test is carried out at a site and an experimental dispersion curve containing N data points is obtained. Each data point consists of a frequency, f_i, and a phase velocity, V_i^{obs}. To initiate the inversion process, an initial profile with M assumed layers, $\mathbf{p}^0$, is assumed. Mathematically, $\mathbf{p}^0$ is a vector whose elements, p_j^0, represent the shear wave velocity and/or thickness of each layer. The initial profile, $\mathbf{p}^0$, is then utilized to calculate the theoretical phase velocity, V_i^{thr}, at each frequency, f_i. The objective of inversion is to find a vector which minimizes the difference between the theoretical and observed data.

Since the inverse problem is linearized, several iterations are necessary before the final profile is obtained. This procedure is described below.

The initial profile, $\mathbf{p}^0$, is utilized to calculate the theoretical phase velocity, V_i^{thr}, and the partial derivatives, $\partial V_i^{thr}/\partial p_j^0$ at each frequency. The governing equations of the inverse problem can then be expressed as

$$V_i^{obs} - V_i^{thr} = \sum_{j=1}^{K} \frac{\partial V_i^{thr}}{\partial p_j} \Delta p_j \qquad i = 1, \ldots, N \tag{5.1}$$

or in matrix form

$$A\Delta p = \Delta c \tag{5.2}$$

where

$\Delta \mathbf{c}$ = $(\Delta c_1, \Delta c_2, \ldots, \Delta c_N)^T$ where $\Delta c_i = V_i^{obs} - V_i^{thr}$.

$\Delta \mathbf{p}$ = $(\Delta p_1, \Delta p_2, \ldots, \Delta p_K)^T$ is defined as a correction or modification vector which is added to vector $\mathbf{p}^0$ to form a new vector of unknowns $\mathbf{p}^i$ for the next iteration. In the vector,

K = M, if layer thicknesses are fixed,

K = 2M - 1, if both shear wave velocity and thickness of each layer need to be determined simultaneously.

$\mathbf{A}$ = N x K matrix of partial derivatives whose elements $A_{ij} = \partial V_i^{thr}/\partial p_j^o$.

Vector $\mathbf{p}^i$ is considered as the solution to the unknowns when vector $\Delta \mathbf{c}$ in Eq. 5.2 is sufficiently small. This is elaborated in the next section.

The choice of the number of experimental dispersion data points (parameter N above) depends on the quality of the field data and the number of unknowns (parameter K) in the trial profile. In practice, it is assumed that N (number of dispersion data points) is greater than K (number of unknowns). Thus, the problem defined by Eq. 5.2 is overconstrained. Typically, parameter N is limited to 20 to 50 data points. As indicated before, parameter M is limited to five when both layer thickness and stiffness are to be determined, and is about 10 when only stiffness is to be determined.

In general, Eq. 5.2 cannot be solved through calculating the conventional inverse of matrix $\mathbf{A}$, $\mathbf{A}^{-1}$. Matrix $\mathbf{A}^{-1}$ exists only if $\mathbf{A}$ is square and non-singular. An approach to solving Eq. 5.2 is to construct its normal or Gaussian-Newton equation. This results in the classical least-squares solution

$$\Delta p = (A^T A)^{-1} A^T \Delta c \tag{5.3}$$

subject to minimization of $(\Delta \mathbf{c} - \mathbf{A}\Delta \mathbf{p})^T(\Delta \mathbf{c} - \mathbf{A}\Delta \mathbf{p})$ with respect to $\Delta \mathbf{p}$. This solution is also known as the optimization solution.

The computation of matrix $\mathbf{A}^T\mathbf{A}$ may involve numerical inaccuracy which can be troublesome when the number of dispersion data or the number of layers are large. To avoid this drawback,

the singular value decomposition of a matrix (Golub and Reinsch, 1970) approach has been utilized to construct the generalized inverse solution of Eq. 5.2.

The decomposition of matrix **A** leads to a product of three matrices

$$A = USV^T \tag{5.4}$$

where

U = N X K matrix whose columns are eigenvectors, $\mathbf{u}_j$ (j = 1, ..., K), of length N associated with the columns (observations) of **A**,

V = K X K matrix whose columns are eigenvectors, $\mathbf{v}_j$ (j = 1, ..., K), of length K associated with the rows (parameters) of **A**, and

S = K X K diagonal matrix with diagonal entries, s_{jj} (j = 1, ..., K), which are the non-negative square roots of the eigenvalues of symmetric matrix $\mathbf{A}^T\mathbf{A}$ and known as the singular values of **A**.

By substituting Eq. 5.4 into Eq. 5.3 and utilizing the orthonormal property of **U** and **V** [i.e. $\mathbf{U}^T\mathbf{U} = \mathbf{V}^T\mathbf{V} = \mathbf{V}\mathbf{V}^T = \mathbf{I}$ (unit matrix)], it is easy to show that

$$\Delta p = VS^{-1}U^T\Delta c \tag{5.5}$$

This expression gives the generalized inverse solution of Eq. 5.2.

Adding $\Delta\mathbf{p}$ to $\mathbf{p}_0$ yields an updated profile from which a set of new phase velocities and a set of new partial derivatives can be calculated. This procedure is repeated until Δc_i's (elements of vector $\Delta\mathbf{c}$ described in Eq. 5.2) are sufficiently small. At this time, a profile which satisfies the given data is found.

The convergence of successive iterations is monitored by the following root-mean-squares (RMS) error criterion,

$$\varepsilon = \sqrt{\frac{1}{N}\sum_{i=1}^{N}\Delta c_i} \tag{5.6}$$

The iteration procedure is terminated when ε reaches an small value or when all elements of vector $\Delta\mathbf{c}$ are within the standard error bounds of each experimental datum or other pre-specified limits.

In many applications, a physically acceptable shear wave velocity profile can not be simply determined from Eq. 5.5 due to the lack of numerical stability; that is, a small change in the data can lead to an unacceptably large change in the derived profile. The remedy to this problem is as follows.

Let us re-write Eq. 5.5 in the form of a linear combination or weighted sum of eigenvectors, $\mathbf{v}_j$

$$\Delta p = \sum_{j=1}^{K} \frac{u_j^T \Delta c}{s_j} v_j \tag{5.7}$$

Vectors $\mathbf{v}_j$ are finite in magnitude and increasingly oscillatory as j increases. Hence, the stability of the solution is controlled by the magnitude of $\mathbf{u}_j^T\Delta\mathbf{c}/s_{ij}$. As j increases, s_{ij} becomes significantly smaller than $\mathbf{u}_j^T\Delta\mathbf{c}$. This can result in very large numbers and cause instability in the solution. To remedy this problem, the singular value decomposition algorithm has been combined with Marquardt's technique (Jupp and Vozoff, 1975). In this approach, s_{ij} in Eq. 5.7 is replaced by $(s_{ij} + \gamma/s_{ij})$. The solution can then be written as

$$\Delta p = \sum_{j=1}^{K} \frac{s_{jj}}{s_{jj}^2 + \gamma} u_j^T \Delta c \; v_j \tag{5.8}$$

where γ is a "small" (in comparison with the largest singular value) positive number. Parameter γ, known as Marquardt's factor, dampens or eliminates the undesirable effects which small singular values can have on the solution.

Evaluation of Uncertainty

In addition to the representative shear wave velocity profile, the level of uncertainty associated with each derived layer parameter also needs to be estimated. To evaluate uncertainty in the profile, the variance of each individual parameter is determined according to the statistics of experiment errors. By taking into account the stability constraints shown in Eq. 5.8, the variance of each parameter can then be estimated through the following formulation:

$$Var[\Delta p_j] = \sigma^2 \sum_{k=1}^{K} \left[V_{jk} \frac{s_k}{(s_k^2 + \gamma)} \right]^2 \tag{5.9}$$

where V_{jk} are the elements of matrix $\mathbf{V}$, and σ^2 is associated with the random errors in the experimental data. The approximate value of σ^2 is given by (Draper and Smith, 1981)

$$\sigma^2 = \frac{1}{N - K} (\Delta c - A\Delta p)^T (\Delta c - A\Delta p) \tag{5.10}$$

The square root of each variance gives the standard error of the corresponding profile parameter.

It should be pointed out that the uncertainty estimated in this way is only related to the random error in the experimental data. Other factors, such as errors in the assumed profile (Poisson's ratio and mass density), simplifying assumptions in the algorithm, and systematic errors in the data, are not included. Therefore, the estimation should be considered as the lower limits of the level of uncertainty.

Sensitivity Analysis

In this section, examples from the analysis of a set of synthetic dispersion data are presented to illustrate the applicability and limitation of the inversion process presented. The data corresponds to a three-layer system of pavement type. The system consists of a 75 mm-thick AC layer (shear wave velocity of 900 m/sec) over a 150 mm-thick base (shear wave velocity of 600 m/sec) and subgrade (shear wave velocity of 300 m/sec). A Poisson's ratio of 0.33 and a uniform mass density were assigned to each layer.

Phase velocities were calculated at twenty one frequencies using the layer properties described above. These "data" were then input to the inversion program to backcalculate the shear wave velocity profile.

As the data are theoretically calculated, they are not contaminated with systematic errors or random scatter usually contained in the field data. The same theoretical algorithm used for calculating the dispersion curve was used as a subroutine in the inversion program. In addition, the exact properties of each layer are known. As such, any differences between the true and backcalculated profiles are due to the weaknesses of the inversion algorithm.

Different trial initial profiles were used to examine the convergence by comparing the "observed"[1] and the "final"[2] dispersion curves in the following simulations. In almost all instances, the same results were achieved. However, a reasonable setup of the initial profile is important to reduce the computation time.

Simulation 1

In this simulation, it was assumed that the number and thicknesses of layers were known. Only shear wave velocity for each layer had to be determined. The trial and backcalculated profiles are shown in Table 5.1. The backcalculated profile is identical to the true profile. For each data point at a given wavelength, the percent data misfit is calculated by simply determining the relative errors between the observed and final dispersion data, $\Delta c_i/V_i^{obs}$. The maximum, minimum, and average misfit amongst the 21 data points are also given in Table 5.1. The complete convergence in data matching after backcalculation demonstrates the effectiveness and accuracy of the process.

The same exercise with the same trial profile but using less data points were repeated. The results obtained were the same as those given in Table 5.1.

---

[1] for simplicity, the synthetic dispersion curve will be called the "observed" dispersion curve.

[2] the "final" dispersion curve refers to the dispersion curve obtained from the profile after the completion of inversion

Table 5.1 - Inversion for shear wave velocity only when layer thicknesses are correct and fixed

Layer Number	Thickness (mm)	Shear Wave Velocity (m/s)		
		True	Trial	Backcalculated
1	75	900	750	900
2	150	600	450	600
3	-	300	200	300

Data misfit (%): Min = 0.0, Max = 0.0, Average = 0.0.

Simulation 2

In this simulation, it was assumed that only the number of layers was known. Shear wave velocity for each layer was backcalculated with the arbitrarily fixed layer thicknesses. The trial and backcalculated profiles are shown in Table 5.2. At a first sight, the differences between the true and backcalculated shear wave velocities may seem small. However, as indicated before, the dispersion data used in the inversion process are "accurate" (i.e. error and scatter free). Therefore, the differences are rather significant. This emphasizes that, similar to any other NDT method, in order to obtain an accurate stiffness profile, the thickness of the layers should be accurately known.

The observed and final dispersion data are compared in Fig. 5.1. The two dispersion curves deviate from one another significantly. The maximum misfit is more than 8 percent.

Table 5.2 - Inversion for shear wave velocity only when layer thicknesses are incorrect and fixed

Layer Number	Thickness (mm)		Shear Wave Velocity (m/s)		
	True	Trial	True	Trial	Backcalculated
1	75	90	900	750	888
2	150	120	600	450	570
3	-	-	300	200	333

Data misfit (%): Min = 0.06, Max = 8.20, Average = 1.16.

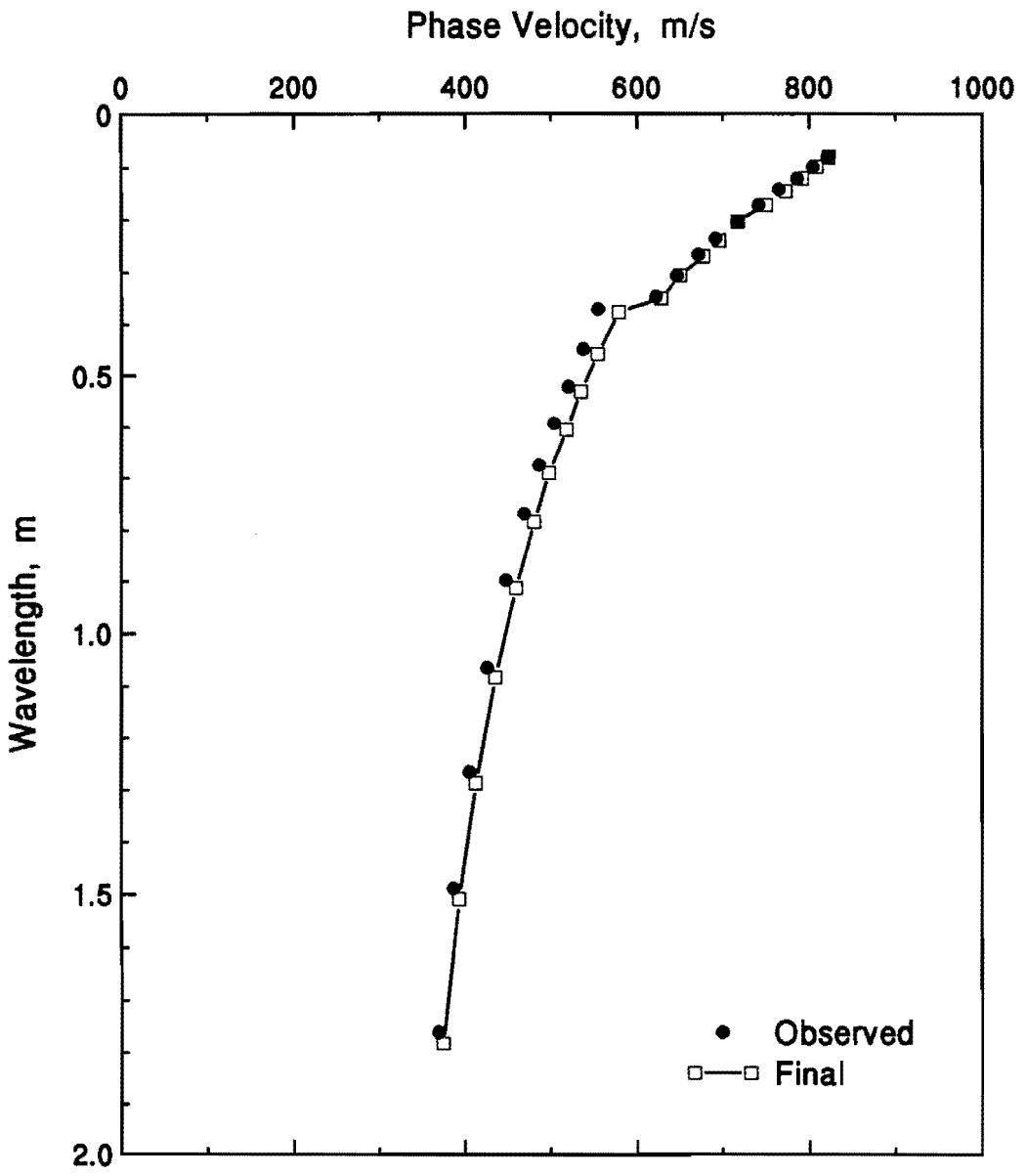

Fig. 5.1 - Comparison of observed and final dispersion curves

Simulation 3

In this simulation, the same trial velocities and layer thicknesses used in Simulation 2 were utilized. However, both thickness and shear wave velocity for each layer were determined through the inversion process. The results from this simulation are listed in Table 5.3. Once again, the thicknesses and velocities are accurately determined. The mismatch between the observed and final dispersion curves is practically zero. The results obtained in this simulation demonstrate the effectiveness and accuracy of the inversion process.

Table 5.3 - Inversion for both layer thickness and shear wave velocity

Layer Number	True		Trial		Backcalculated	
	h (mm)	Vs (m/s)	h (mm)	Vs (m/s)	h (mm)	Vs (m/s)
1	75	900	90	750	75	900
2	150	600	120	450	150	600
3	-	300	-	200	-	300

Data misfit (%): Min = 0.02, Max = 0.08, Average = 0.05.

Simulation 4

This simulation corresponds to a situation usually encountered in practice. It was assumed that thicknesses, and shear wave velocities of layers, as well as the number of layers are all unknown. Thicknesses and shear wave velocities were estimated by assuming that the profile contains five layers. The thicknesses of layers in the trial profile were assumed to be equal.

The final profile after inversion is included in Table 5.4 and is compared with the true profile in Fig. 5.2. The thickness and velocity of the surface layer are determined relatively accurately. The thickness of the second layer of the true profile is determined accurately, provided that the second and third layers of the backcalculated profile are combined. This is justified because the velocities of the second and third layers of the final profile are rather close. The velocity of the half space is predicted rather well, if the fourth layer is ignored.

The velocity of the fourth layer from the final profile is significantly higher than the actual value. This discrepancy can be attributed to the change in the branch patters (five layers against three layers) in dispersion curves. This corresponds to one of the weaknesses of the present inversion process.

Simulation 5

In every simulation represented up to this point, the results were obtained based on the assumption that the Poisson's ratio and density for each layer are known. The effects of mis-estimation of Poisson's ratio on backcalculated profile are demonstrated here.

Table 5.4 - Inversion for both layer thickness and shear wave velocity with incorrect number of layers

Layer Number	True		Trial		Backcalculated	
	h (mm)	Vs (m/s)	h (mm)	Vs (m/s)	h (mm)	Vs (m/s)
1	75	900	75	750	77	890
2	150	600	75	600	27	646
3	-	300	75	450	121	608
4	-	-	75	300	36	351
5	-	-	-	200	-	289

Data misfit (%): Min = 0.35, Max = 2.18, Average = 1.26.

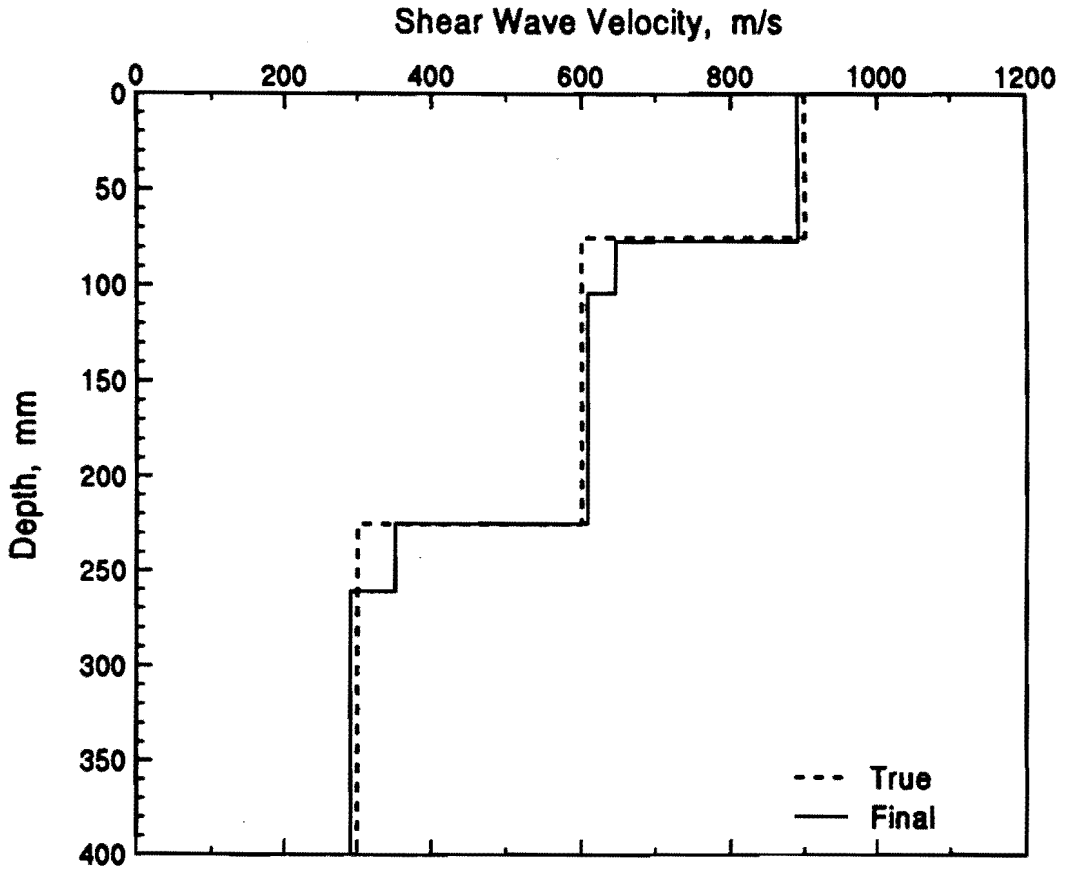

Fig. 5.2 - Comparison of true and final shear wave velocity profile

A Poisson's ratio of 0.25, rather than 0.33, was assumed for all layers. For simplicity, the number and thicknesses of layers have been assumed to be known parameters. The backcalculated velocities are shown in Table 5.5.

Decreasing the Poison's ratio from 0.33 to 0.25 should naturally result in an average increase of about 1.5 percent in shear wave velocity of each layer. It can be seen that velocities of all layers are predicted closely. This confirms that Poisson's ratio has a minor influence on dispersion and the backcalculated results from dispersion data.

Table 5.5 - Inversion for shear wave velocity with incorrect Poisson's ratio

Layer Number	Thickness (mm)	Shear Wave Velocity (m/s)		
		True	Trial	Backcalculated
1	75	900	750	902
2	150	600	450	628
3	-	300	200	301

Data misfit (%): Min = 0.51, Max = 3.63, Average = 1.45.

Chapter 6

Seismic Pavement Analyzer

Since the Seismic Pavement Analyzer can be easily utilized to collect the SASW data, it is beneficial to describe the device and its features.

The Seismic Pavement Analyzer (SPA) is an instrument designed and constructed to monitor conditions associated with pavement deterioration. It measures such conditions as voids or loss of support under a rigid pavement, moisture infiltration in asphalt concrete pavement, fine cracking in pavements, delamination of overlays, and aging of asphalt.

The SPA detects these pavement conditions by estimating compression and/or shear wave velocities in the pavement, base, and subgrade from the following wave propagation measurements: 1. Impact Echo (IE), 2. Impulse Response (IR), 3. Spectral Analysis of Surface Waves (SASW), 4. Ultrasonic Surface Waves (USW), and 5. Ultrasonic Body Waves (UBW).

The SPA records the pavement response produced by high- and low-frequency pneumatic hammers on five accelerometers and three geophones. A computer controls data acquisition, instrument control, and interpretation; measurements and interpretations are reported in both screen and database formats.

The equipment can perform several functions: 1. analyzing in detail pavement conditions identified in the network-level surveys; 2. diagnosing specific distress precursors to aid in selecting the maintenance treatment; and 3. monitoring pavement conditions after maintenance to determine the treatment's effectiveness.

The operating principle of the SPA is based on generating and detecting stress waves in a layered medium. Each of the five tests and its areas of strength are summarized in Table 6.1. The SASW method was discussed in the previous chapters, and therefore, not discussed any further. The design and construction of the SPA are based on two general principles. First, the strength of each method should be fully utilized; and second, testing should provide enough redundancy to identify each layer that will potentially contribute to the distress of the pavement.

The ultrasonic-body-wave method can determine the existence of cracks, even if they have not extended through the thickness of the layer. In this method, stress wave energy is generated at one point and detected at several other points. Any cracks in the material located between the source and the receiver will delay the direct propagation of waves and will reduce the amplitude associated with the arriving wave. Differentiation between a strong material containing cracks and a weak material is not possible at this time.

Table 6.1 - Strengths of five testing techniques used by Seismic Pavement Analyzer

Testing Technique	Strengths
Ultrasonic Body Wave	Young's Modulus of top paving layer
Ultrasonic Surface Wave	Shear modulus of top paving layer
Impulse Response	Modulus of subgrade reaction of foundation layers
Spectral Analysis of Surface Waves	Modulus of each layer Thickness of each layer Variation in modulus within each layer
Impact Echo	Thickness of paving layer or depth to delaminated layer

A void beneath or within a slab results in increased flexibility of the slab. Therefore, measuring the flexibility of the slab at different locations using the impulse-response method can pinpoint the voids or loss of support. Initial stages of debonding may not significantly affect the results from the IR method.

The impact echo method distinguishes between overlay delamination and voids beneath or within the slab. The method, a special case of ultrasonic-body-wave propagation, can determine the depth to the reflector.

The impulse response and the impact echo are the prime methods for determining the location and existence of delamination. The theoretical and experimental aspects of using these two tests for detecting overlay delamination are identical to those used for locating voids and loss of support. The only differences are the nature and location of the interface. For delamination, the void occurs at the interface of two layers and the delaminated layer is located closer to surface.

Description of Measurement Technologies

Impulse-Response (IR) Method

Two parameters are obtained with the IR method — the shear modulus of subgrade and the damping ratio of the system. These two parameters characterize the existence of several distress precursors. In general, the modulus of subgrade can be used to delineate between good and poor support. The damping ratio can distinguish between the loss of support or weak support. The two parameters are extracted from the flexibility spectrum measured in the field. An extensive theoretical and field study (Reddy, 1992) shows that, except for thin layers (less than 75 mm) and soft paving layers (i.e., flexible pavements), the modulus obtained by the IR method is a good representation of the shear modulus of subgrade, with little influence from the stiffness of the paving layers. In other cases, the properties of the pavement layers (AC and base) affect the outcome in such a manner that the modulus obtained from the IR test should be considered an overall modulus.

The IR tests use the low-frequency source and geophone G1 (see Fig. 6.1). The pavement is impacted to couple stress wave energy in the surface layer. At the interface of the surface layer and the base layer, a portion of this energy is transmitted to the bottom layers, and the remainder is reflected back into the surface layer. The imparted energy is measured with a load cell. The response of the pavement, in terms of particle velocity, is monitored with the geophone and then numerically converted to displacement. The load and displacement time-histories are simultaneously recorded and are transformed to the frequency domain using a Fast-Fourier Transform algorithm. The ratio of the displacement and load (termed flexibility) at each frequency is then determined.

For analysis purposes, the pavement is modeled as a single-degree-of-freedom (SDOF) system. Three parameters are required to describe such a system — natural frequency, damping ratio, and gain factor. The last two can be replaced by the static flexibility and the peak flexibility. These three parameters are collectively called the modal parameters of the system. The natural frequency and gain factor are used to determine the modulus of subgrade. The damping ratio is used directly.

To determine the modal parameters, a curve is fitted to the flexibility spectrum according to an elaborate curve-fitting algorithm that uses the coherence function as a weighing function (Richardson and Formenti, 1982). The poles, zeros, and gain factor obtained from the curve-fitting are easily converted to modal parameters. From these parameters, the modulus of subgrade is determined. The shear modulus of subgrade, G, is calculated from (Dobry and Gazetas, 1986)

$$G = (1 - \nu) / [2L\, A_o\, I_s\, S_z] \qquad (6.1)$$

where ν = Poisson's ratio of subgrade, L = length of slab, and A_o = static flexibility of slab (flexibility at f = 0). The shape factor, S_z, has been developed by Dobry and Gazetas (1986). I_s (Nazarian et al., 1994) is a parameter which considers the effect of an increase in flexibility

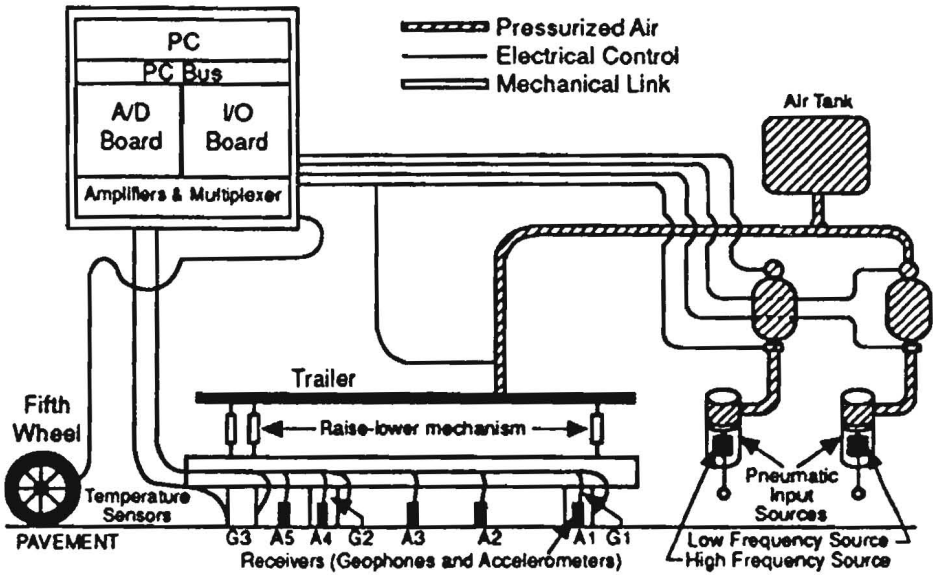

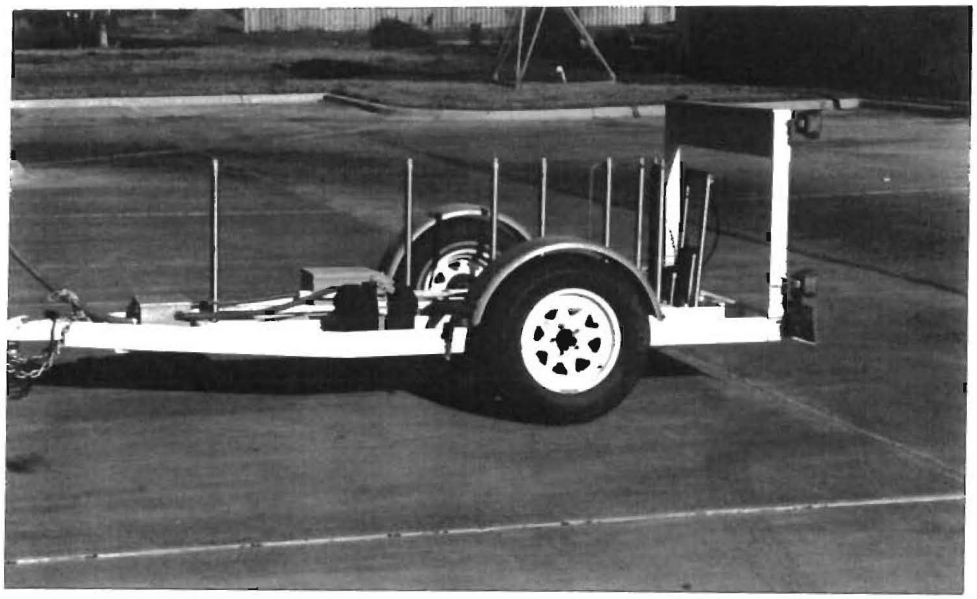

Fig. 6.1 - Seismic Pavement Analyzer

near the edges and corners of a slab. Parameter I_s is a function of the length and width of the slab, as well as the coordinates of the impact point relative to one corner. Depending on the size of the slab and the point of impact, the value of I_s can be as high as 6.

The damping ratio, which typically varies between 0 to 100 percent, is an indicator of the degree of the slab's resistance to movement. A slab that is in contact with the subgrade or contains a water-saturated void demonstrates a highly damped behavior and has a damping ratio of greater than 70 percent. A slab containing an edge void would demonstrate a damping ratio in the order of 10 to 40 percent. A loss of support located in the middle of the slab will have a damping of 30 to 60 percent.

Ultrasonic-Surface-Wave Method

The ultrasonic-surface-wave method is an offshoot of the SASW method. The major distinction between these two methods is that in the ultrasonic-surface-wave method the shear velocity of the top paving layer can be easily and directly determined without a complex inversion algorithm. To implement the method, the high-frequency source and accelerometers A2 and A3 (see Fig. 6.1) are utilized.

At wavelengths less than or equal to the thickness of the uppermost layer, the velocity of propagation is independent of wavelength. Therefore, if one simply generates high-frequency (short-wavelength) waves, and if one assumes that the properties of the uppermost layer are uniform, the shear wave velocity of the upper layer, V_s, can be determined from

$$V_s = (1.13 - 0.16\nu)\, V_{ph} \tag{6.2}$$

The shear modulus of the top layer, G, can alternatively be determined from

$$G = \rho\, V_s^2 \tag{6.3}$$

where V_{ph} = velocity of surface waves, ρ = mass density, and ν = Poisson's ratio.

The methodology can be simplified even further. If one assumes that the properties of the uppermost layer are uniform, the shear wave velocity of the top layer can be determined from

$$V_s = (1.13 - 0.16\nu)(\, m/360D) \tag{6.4}$$

Parameter m (deg/Hz) is the least-squares fit slope of the phase of the transfer function in the high-frequency range.

Ultrasonic Compression Wave Velocity Measurement

Theoretically, all accelerometers can be used to measure compression wave velocity of the upper layer of pavement. Once the compression wave velocity of a material is known, its Young's modulus can be readily determined.

Miller and Pursey (1955) found that when the surface of a medium is impacted, the generated stress waves propagate mostly with Rayleigh wave energy and, to a lesser extent, with shear and compression wave energy. As such, the body wave energy present in a seismic record generated using the set-up shown in Fig. 6.1 is very small; for all practical purposes it does not contaminate the SASW results. However, compression waves travel faster that any other type of seismic wave, and are detected first on seismic records.

An automated technique for determining the arrival of compression waves has been developed. Times of first arrival of compression waves are measured by triggering on an amplitude range within a time window (Willis and Toksoz, 1983).

Impact-Echo Method

The impact-echo method can effectively locate defects, voids, cracks, and zones of deterioration within concrete. The method has been thoroughly studied and effectively used on many projects by researchers at the National Institute of Standards and Technology. In a comprehensive theoretical and experimental study, Sansalone and Carino (1986) considered the effects of type of impact source, distance from impact point to receiver, type of receiving transducers, and depth of reflecting interfaces.

The high-frequency source and accelerometer A1, are used, and possibly A2 as well (see Fig. 6.1). Once the compression wave velocity of concrete, V_p, is known, the depth-to- reflector, T, can be determined from (Sansalone and Carino, 1986)

$$T = V_p / 2f \tag{6.5}$$

where f is the resonant (return) frequency obtained by transforming the deformation record into the frequency domain.

DATA COLLECTION AND ANALYSIS

Data Collection

The technician initiates the testing sequence through the computer, that then lowers the sensors and impact unit onto the pavement surface. The high-frequency source is then activated. The outputs of the three accelerometers closest to the high-frequency source, as well as the load cell connected to this source, are used first. The source is fired four to seven times. For the last three impacts of the source, the output voltages of the load cell and the receivers are saved and averaged (stacked) in the frequency domain. The other (prerecording) impacts are used to adjust

the gains of the pre-amplifiers. The gains are set in a manner that optimizes the dynamic range. After this step, another set of impacts are utilized to determine compression wave velocities. To perform the test, the gains of all amplifiers are set to maximum. In this manner, the arrival of compression waves can be better identified.

The same procedure is followed again, but the first three accelerometers are replaced by the last three accelerometers. A multiplexer switches the accelerometers. The middle accelerometer (third closest accelerometer to the source) is active in both sets of experiments.

Typical voltage outputs of the load cell and the three near accelerometers are shown in Fig. 6.2a. To ensure that an adequate signal-to-noise ratio is achieved in all channels, signals are normalized to a maximum amplitude of one. In this manner, the main features of the signals can be easily inspected.

In the next phase of data collection, the low-frequency load cell and the three geophones are recorded. The procedure described above for each of the accelerometer banks is utilized. A typical output of the three geophones is shown in Fig. 6.2c in the normalized fashion.

The data collected in this fashion has to be processed using signal processing and spectral analysis. These processes are described in the next section.

Data Reduction

Impulse-Response Method

This method uses the voltage output from the first geophone (the geophone closest to the source, G1) and the low-frequency load cell (see Fig. 6.2c).

The load cell record consists of a half-sine wave approximately 2-msec long. The small reverberation past the actual impact corresponds to the reflection of the wave inside the source assembly. The amplitude of this reverberation is muted so it does not affect the results. The response of the geophone is a steady-state damped response. The slight time delay between the geophone and load cell records is the result of the separation between the source and the receiver.

A detailed description of steps necessary to complete the data reduction can be found in Nazarian et al. (1994). Briefly, the output of the load cell and geophone are transformed into the frequency domain using a Fast-Fourier Transform (FFT) algorithm, obtaining the ratio of the particle velocity and the load at each frequency. This function, the mobility spectrum, is then integrated to obtain the flexibility spectrum. The flexibility spectrum is used to determine the parameters for detecting voids or loss of support.

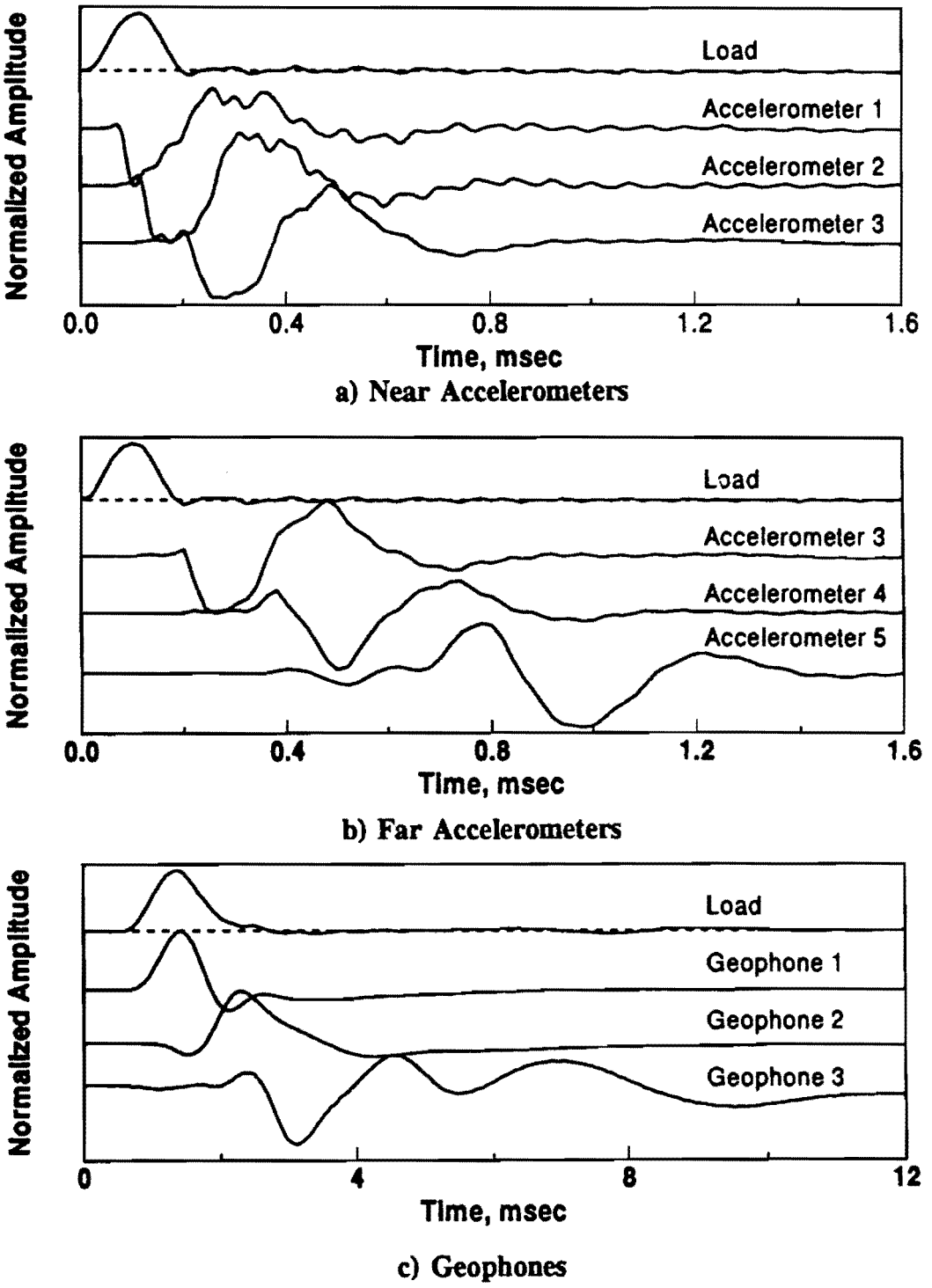

Fig. 6.2 - Typical normalized time records obtained with SPA

A typical flexibility spectrum is shown in Fig. 6.3. The response is as expected, except for frequencies below approximately 50 Hz. The erratic nature of the signal at low frequencies is probably because of the movement of the trailer. This has been minimized in TxDOT SPA.

The coherence function associated with this record is shown in Fig. 6.3b. The coherence values are close to unity except at low frequencies. A coherence value of unity corresponds to a highly coherent signal between the load cell and receiver. In other words, there was no incoherent background noise in the signals.

In the next step, a complex-valued curve representing a single-degree-of-freedom (SDOF) dynamic system is fitted to the flexibility spectrum. A typical fitted curve is shown in Fig. 6.3a. The agreement between the measured and the fitted data is good.

Impact-Echo Method

The impact-echo method is similar to the impulse-response method. However, the impact-echo method uses the records from the small load cell and the accelerometer closest to the high-frequency source. Typical outputs from the accelerometer and the load cell are shown in Fig. 6.2a.

In the next step, the two signals are transformed into the frequency domain following the procedure outlined above for impulse-response testing. A typical frequency-response spectrum for a site is shown in Fig. 6.4a.

The major peak seen in Fig. 6.4a (at about 10 kHz) corresponds to a standing wave within the thickness of the layer and is called the return (resonant) frequency.

The coherence function is shown in Fig. 6.4b. In general, the data collected with the device have no incoherent noise, except at several isolated frequencies.

To calculate the thickness of the layer, the compression wave velocity of the material is determined using the ultrasonic-body-wave method. The thickness is equal to one-half of the ratio between the compression wave velocity and the return resonant frequency.

Ultrasonic-Surface-Wave Method

This method determines the shear wave velocity or shear modulus of the top layer, using the time records of two accelerometers, accelerometer A2 (150 mm away from the source) and accelerometer A3 (300 mm away from the source) (see Fig. 6.2a). These two signals are Fourier-transformed and the ratio of the two signals is calculated in the form of the transfer function. However, unlike the previous two methods, the ultrasonic-surface-wave method uses only the phase of the transfer function. A phase spectrum for time records similar to those shown in Fig. 6.2a is shown in Fig. 6.5a. The phase oscillates on a radius between π and $-\pi$ radians (180 and -180 degrees). This is the standard method of presenting phase data, because the detailed variation in the data can be observed in a small space.

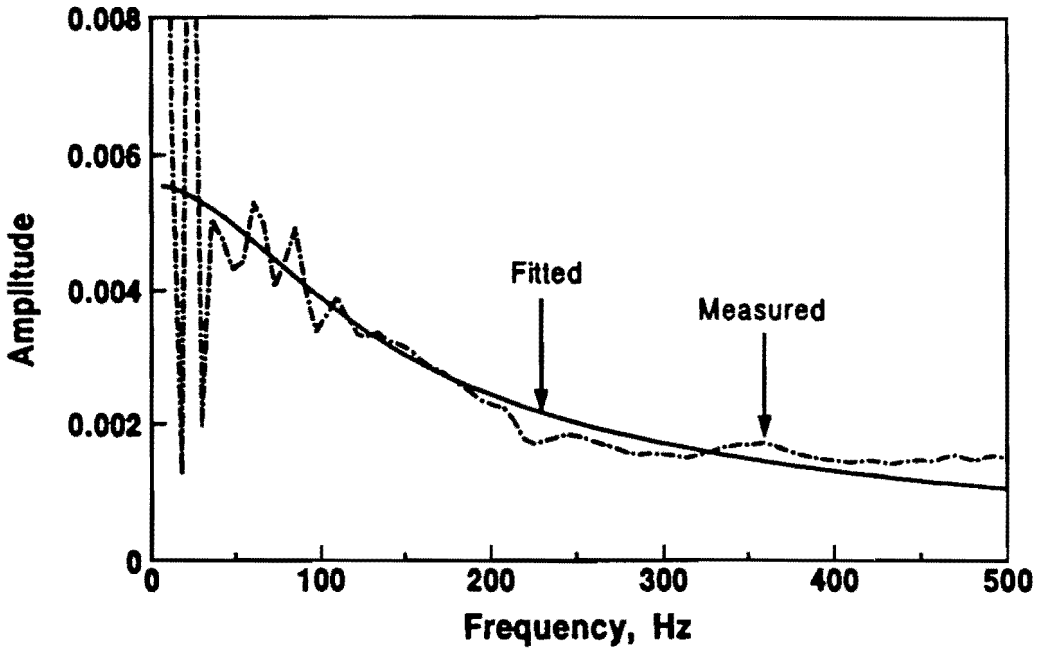

a) Transfer Function

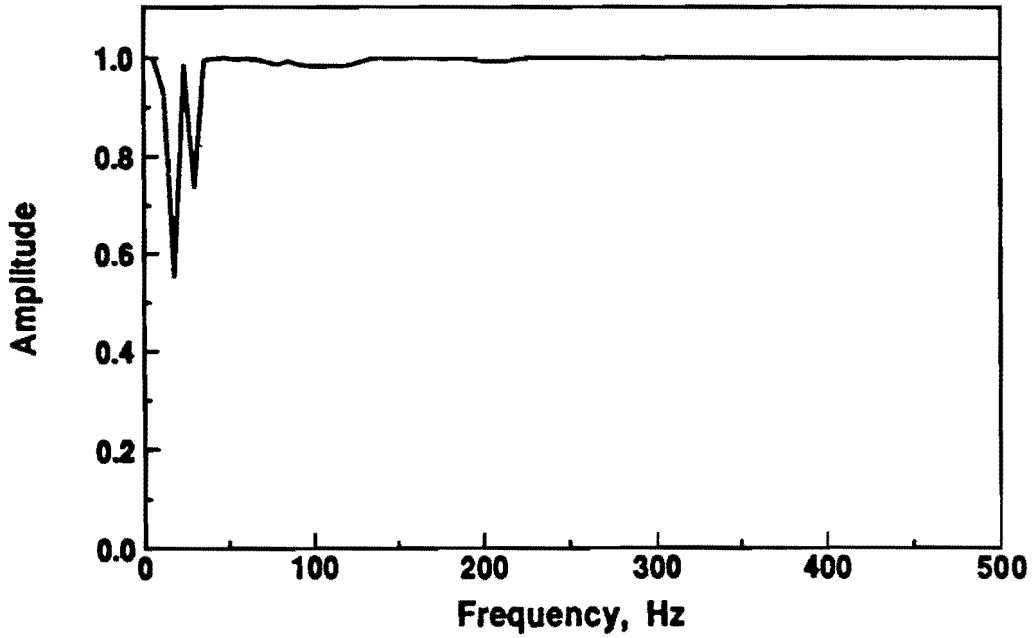

b) Coherence Function

Fig. 6.3 - Typical spectral functions used in impulse-response test

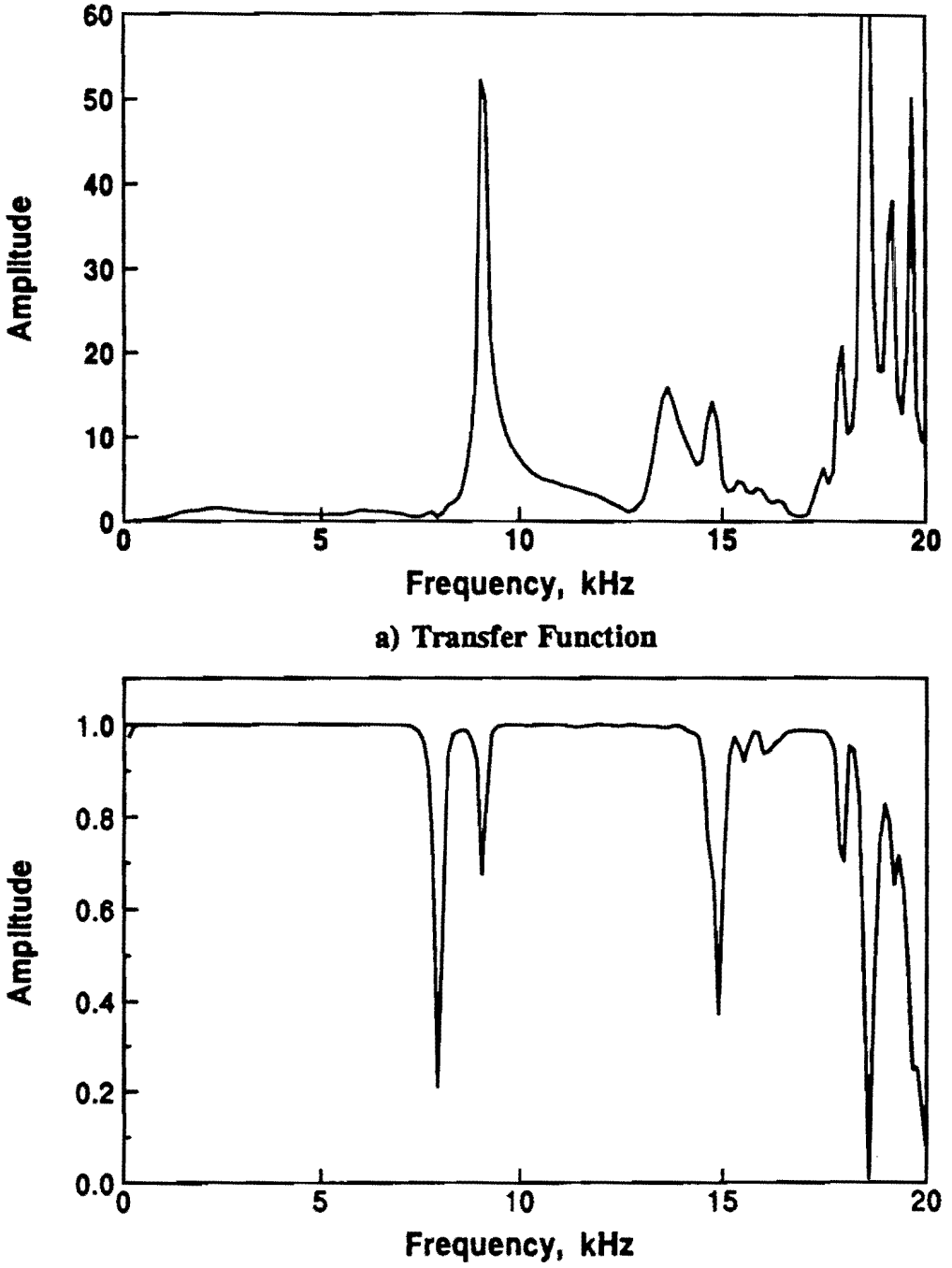

Fig. 6.4 - Typical spectral functions used in impact-echo test

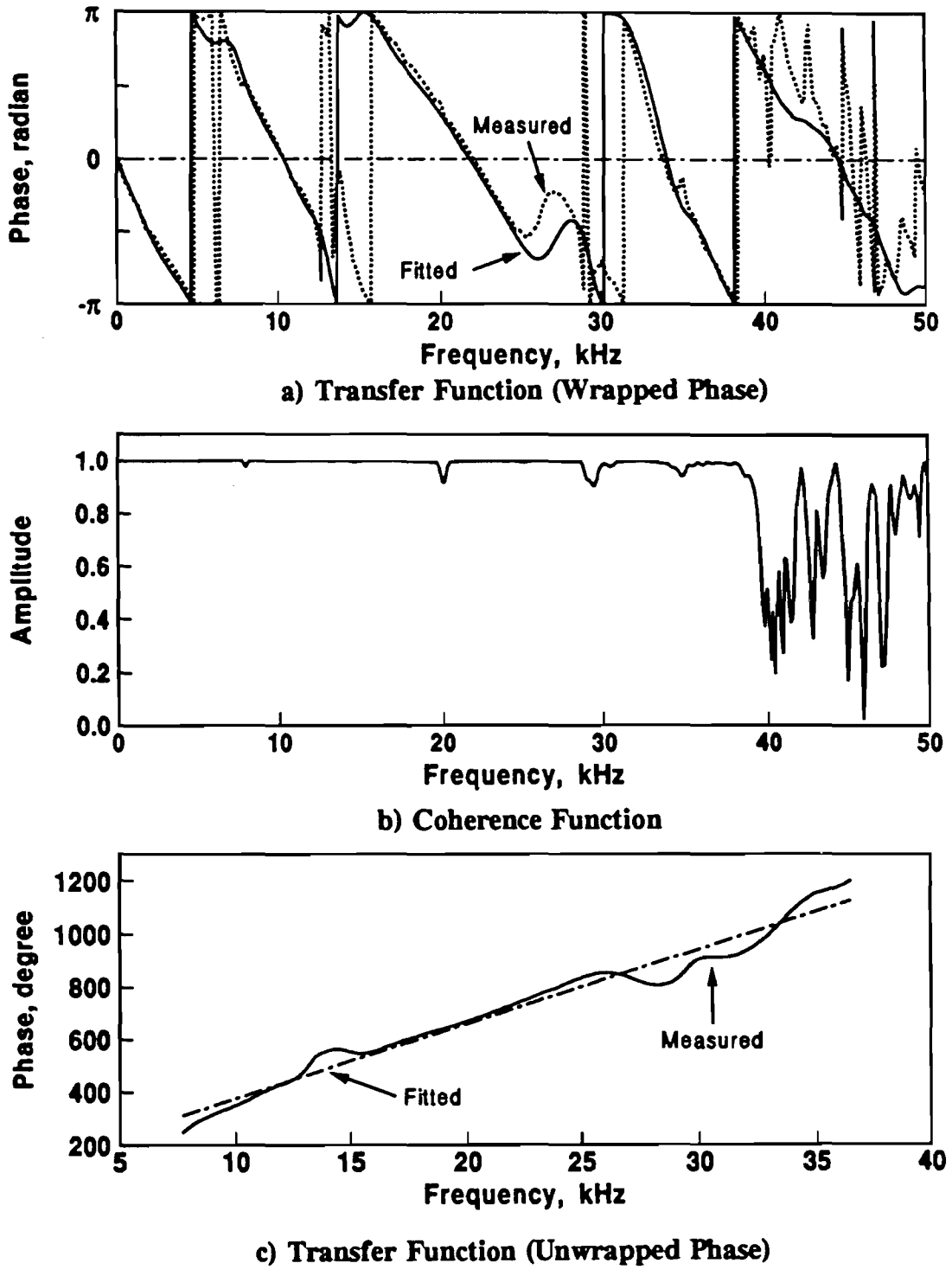

Fig. 6.5 - Typical spectral functions used in ultrasonic-surface-wave test

The data shown in Fig. 6.5a are smooth and do not exhibit much scatter in phase with the frequency, up to a frequency of 35 or 40 kHz. However, the data are rather noisy above a frequency of 35 or 40 kHz.The coherence function associated with this record is shown in Fig. 6.5b. The coherence is almost equal to one, up to a frequency of 35 or 40 kHz. Above the frequency of 35 kHz, the data are of low quality and are not usable.

The frequency of 35 kHz for this experiment corresponds to a wavelength of less than 38 mm. Shorter wavelengths can be investigated using accelerometer A1 and accelerometer A2 (which are spaced 75 mm apart). One physical limitation is the aggregate size. Wavelengths shorter than the maximum aggregate size probably do not follow the laws of wave propagation in a homogeneous medium.

The shear wave velocity of the top layer is obtained using the complex-valued curve-fitting process described in Chapter 3. The results are shown in Fig. 6.5a. The actual and fitted curves compare quite favorably up to a frequency of 30 kHz.

In the next step, the phase is "unwrapped"; that is, the appropriate number of cycles is added to each phase. The unwrapped phase for the "wrapped" phase shown in Fig. 6.5a is shown in Fig. 6.5c. The slope of the line is basically constant with frequency.

Finally, a line is fitted to the curve in the range of frequencies corresponding to wavelengths shorter than the thickness of the top layer. The slope of the line can be used to determine the shear wave velocity (see previous section).

Ultrasonic-Body-Wave Method

The ultrasonic-body-wave method uses the same records as in the ultrasonic-surface-wave method. In Fig. 6.2, the arrival of the compression waves (P-waves) cannot be identified in part because the surface wave energy dominates all signals. To determine the arrival of the P-waves, the gain of all amplifiers is set at the maximum possible range to collect data for determining compression wave velocities. Such a record is shown in Fig. 6.6. Accelerometers A1 and A2 cannot identify the energy associated with the compression waves, because the seismic energy has not traveled over enough distance to separate into distinct compressional and shear waves. However, the other accelerometers, can identify the arrival of the P-waves. In Fig. 6.6, the arrows in each record correspond to the arrival of these waves; typically, accelerometers A3 and A4 record the arrival of energy most consistently. The compression wave velocity is calculated from the distance between the receivers and the difference in the travel time. The compression wave velocity can then be converted to Young's modulus.

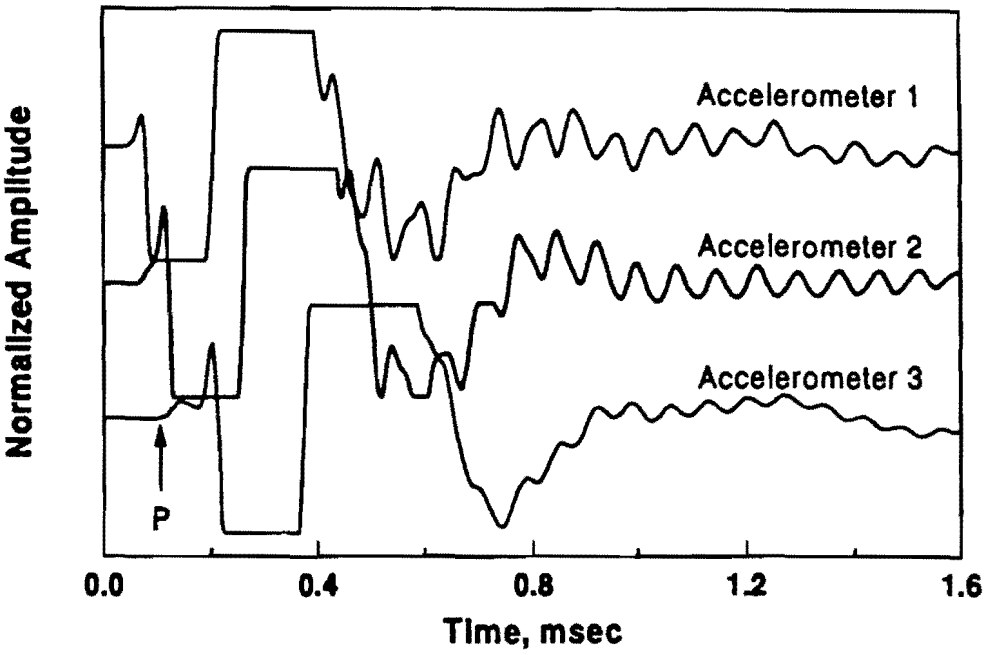

a) Near Accelerometers

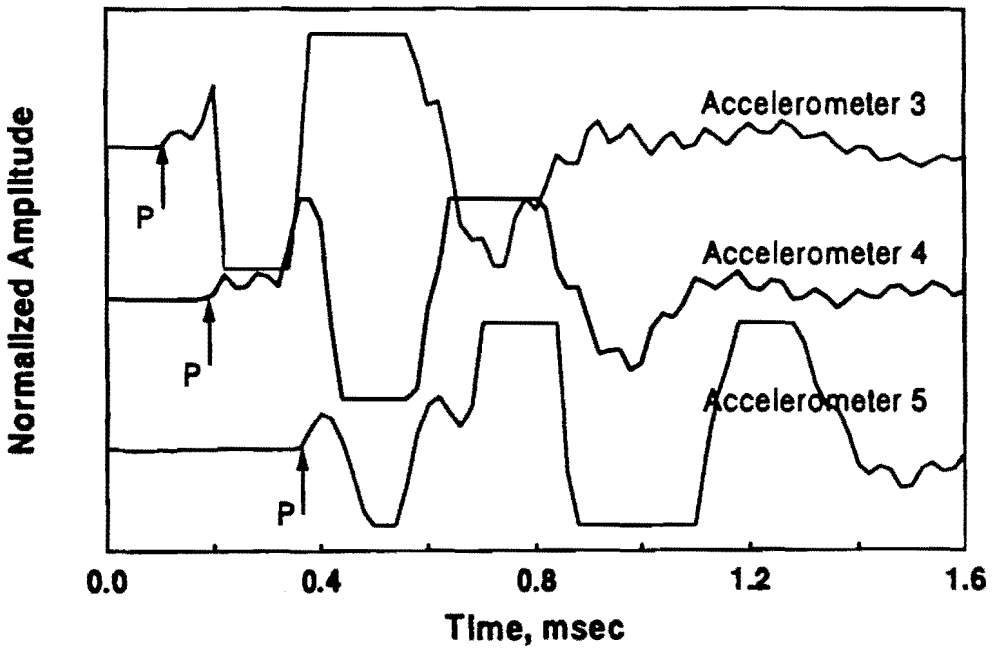

b) Far Accelerometers

Fig. 6.6 - Typical amplified signals used in ultrasonic-body-wave test

Chapter 7

Case Studies

This chapter contains the results from several case studies that demonstrate the effectiveness and limitations of the methods and procedures discussed in the previous chapters. Numerous other case studies were carried out but not repeated for the sake of brevity.

Dispersion data were collected at different pavement sites. The data used in case study 1 were obtained from the conventional manual setup, and the data used in the other case studies were collected with the Seismic Pavement Analyzer.

Case Study 1

A series of tests was carried out at one site on Highway US 69 in Agelina County near Lufkin, Texas. The pavement section reportedly consisted of a 175-mm-thick AC layer. Based on construction drawings, the AC layer consisted of three different lifts placed at different times. The base course consisted of a 250-mm-thick flexible ash base, below which the subgrade existed.

The dispersion curve obtained at this site is shown in Fig. 3.7. Thirty one data points were sampled from the dispersion curve shown in Fig. 3.7 to construct the idealized dispersion curve. The trial profile is shown in Fig. 7.1. The selection of the proper trial profile is rather simple for the top layer and the half-space. A convenient method for determining the trial values for other layers is suggested by Nazarian (1984). The final profile after simultaneous inversion for both layer thickness and shear wave velocity is also presented in Fig. 7.1.

The idealized dispersion curve used in the inversion process is compared with the theoretical one obtained from the backcalculated profile in Fig. 7.2. The two curves compare quite well showing the appropriateness of the backcalculated profile.

The final profile along with the estimated 95 percent confidence interval bounds associated with the shear wave velocity are shown in Fig. 7.3. The confidence interval bounds are rather

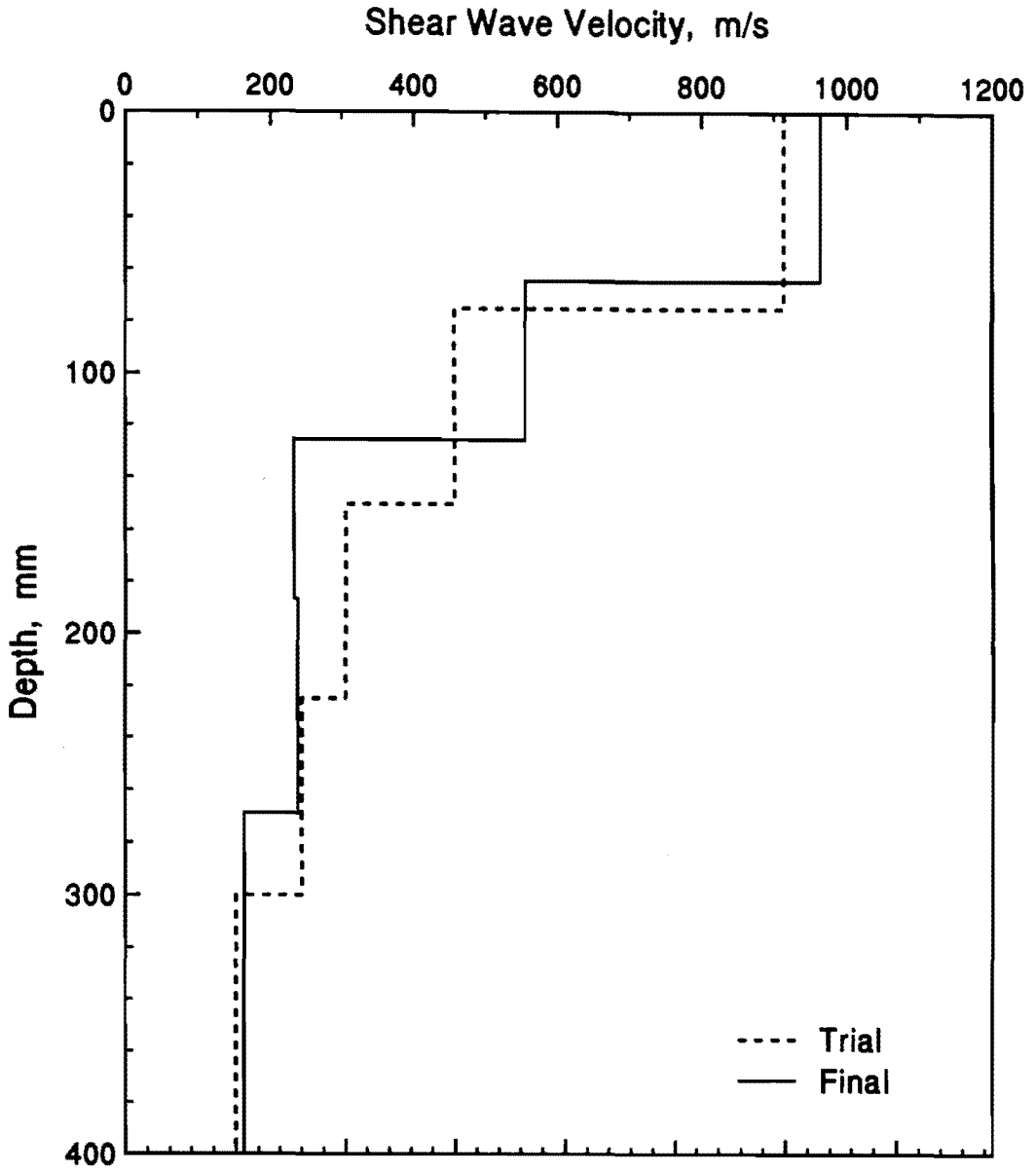

Fig. 7.1 - Trial and final shear wave velocity profiles

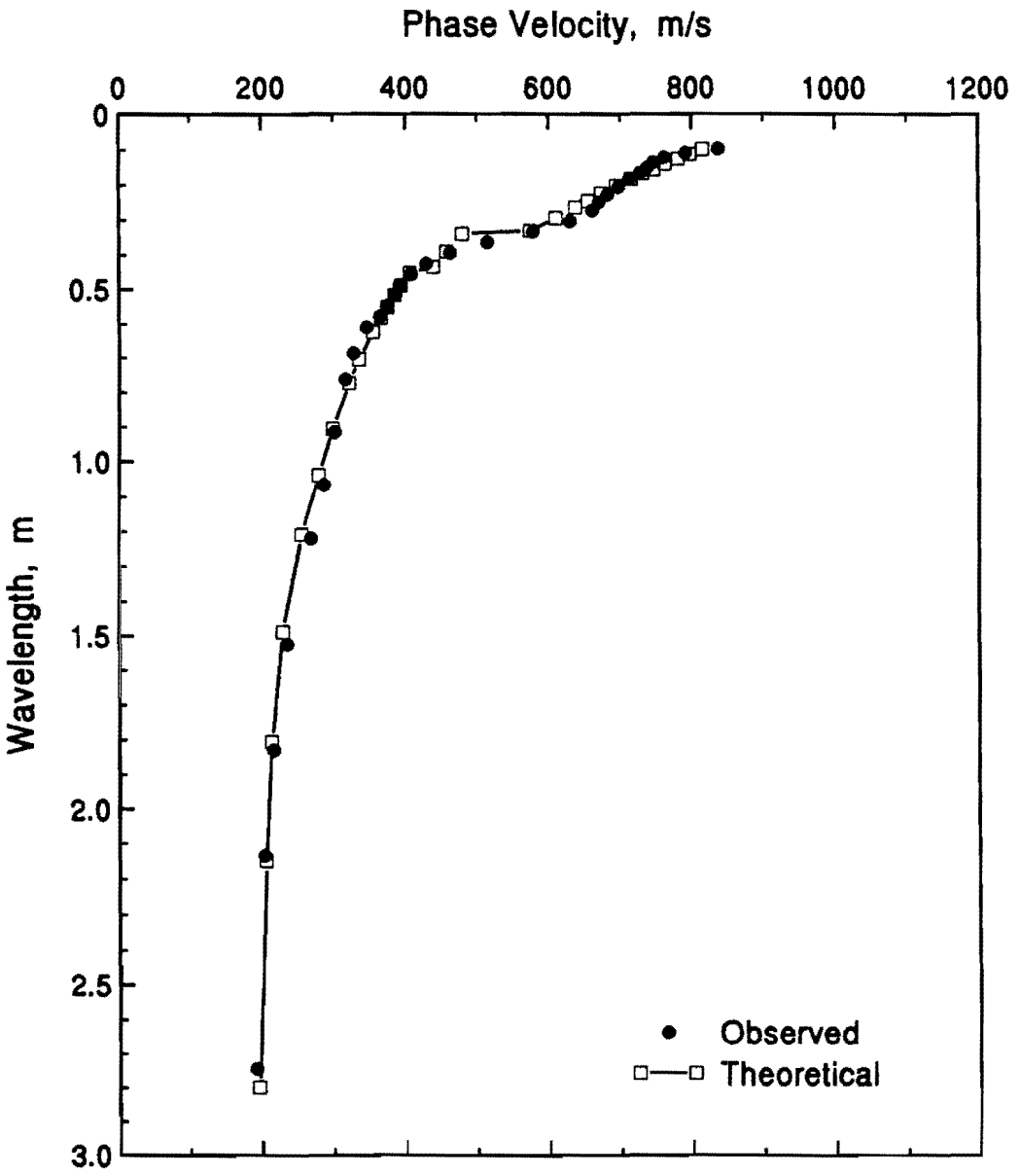

Fig. 7.2 - Comparison of observed and theoretical dispersion curves

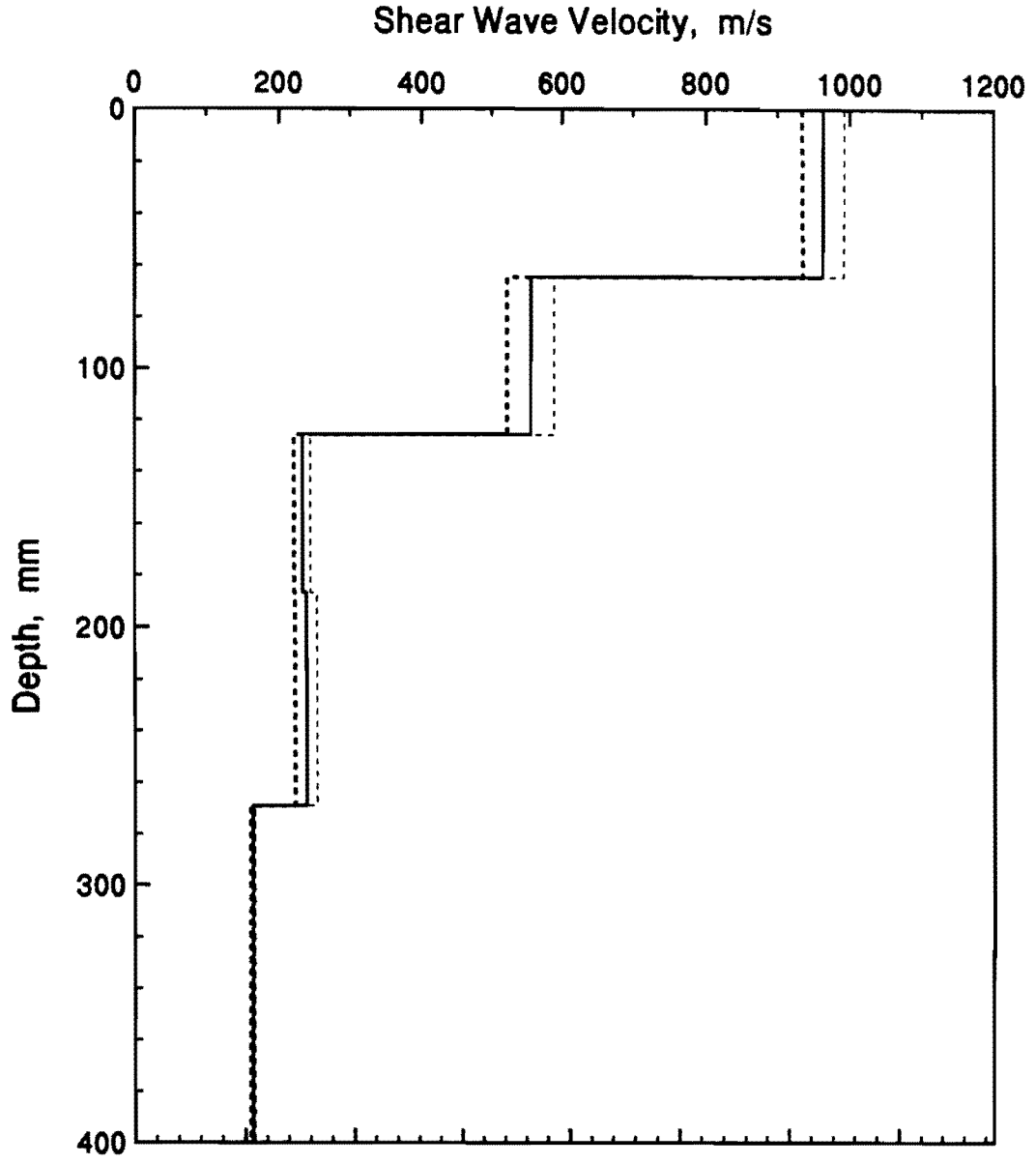

Fig. 7.3 - Final shear wave velocity profile with eatimated error bouds

narrow corresponding to a small scatter in the field data and a good fit between the two dispersion curves.

The thickness of the AC layer is estimated at about 65 mm, underlying a softer layer down to a depth of about 140 mm. The thickness of the base layer was found to be about 150 mm also. As mentioned before, the as-built thickness of the AC layer was reported as 175 mm. Based upon actual coring after the completion of the analysis, it was found that the AC layer was severely stripped. Actually only about 63 mm to 75 mm of the core could be recovered and the rest of the AC layer had lost its binding agent.

The FWD tests were also carried out at the site. A drop load of 45 KN was used. Program MODULUS 4.0 (Uzan et al., 1988) was utilized to backcalculate the moduli. Three different pavement profiles were used. In the first profile, the layering obtained from construction drawings was used. In this case, the thickness of the AC and base were assumed to be 175 mm and 250 mm, respectively. The backcalculated moduli from this layering is reported in Table 7.1. Also shown in the table are the moduli values obtained from SASW tests. The modulus of the subgrade from both methods are quite comparable. However, the moduli of the base and AC layers are quite different. It would be difficult to derive any conclusions from the FWD moduli of the top two layers, because the actual layer thickness were significantly different than those assumed in the backcalculation process.

Table 7.1 - Comparison of Moduli obtained from SASW and FWD methods

Method	Modulus, MPa				
	AC		Base	Subgrade	Absolute Average Error(%)
	Layer 1	Layer 2			
SASW	4,816	1,603	287	147	1.8
FWD (construction Drawings)*	1,351	-	42	147	0.9
FWD (SASW)*	3,500	2,002	28	147	1.3
FWD (coring)*	2,261	1,911	28	147	1.0

* Source for determining layer thickness.

The second profile used was the one obtained from the SASW tests. In this case, the modulus values are much closer. The modulus of base seems unreasonably low (28 MPa). The reason for this matter is unclear.

The third profile used was the one obtained from the actual coring of the site. The thickness of the intact AC layer was reported as 63 mm to 75 mm and the thickness of the base was reported between 150 mm and 175 mm. This profile yields moduli which is similar to that of the SASW profile. This is expected because the layering from the SASW tests and coring are relatively close.

Case Study 2

Tests were carried out at the University of Texas at El Paso (UTEP) Flexible Pavement Facility under controlled conditions. The testing facility as shown in Fig. 7.4 consists of two 6-m by 6-m square pads. One pad consists of 75 mm of asphalt concrete with 150 mm of base over subgrade. The other section consists of 150 mm of AC with 300 mm of base over subgrade. Each test pad is divided into two longitudinal sections. One half is used as the control section. Means of simulating defects are introduced into the other half. The half containing defects is divided into three sections. One of the following defects is introduced into each sections: 1. stripping of the asphalt layer, 2. moisture in the base, and 3. moisture in the base and subgrade.

All paving materials were acquired from vendors approved by the Texas Department of Transportation (TxDOT). All mix designs met the requirements of the TxDOT.

The facility was extensively utilized to determine the accuracy and repeatability of the SASW method. One example of such study is included here.

The effects of change in moisture on the modulus of the base and subgrade were studied. The SASW method was employed to obtain a more comprehensive picture of the facility. Moisture change was achieved by introducing water to the base and subgrade. The amount and pressure of water introduced were carefully controlled with an accurate flow-meter and a pressure regulator.

In the first experiment, water was introduced to the base layer only. SASW tests were performed when the base was wet, dry, and moist. The results for the thick pad are summarized in Table 7.2. The dry condition refers to the natural condition before adding moisture to the base. The moist condition refers to the situation when the change in water content was about 7 percent. The wet condition is the condition when the base was saturated.

Table 7.2 - Variation in Modulus of different layers with moisture when water is added to base

Moisture Condition	Modulus, MPa		
	AC layer	Base	Subgrade
Dry	4594	149	145
Moist*	4281	172	141
Saturated	4033	160	138

* Refers to the case when the change of moisture content was about 7 percent.

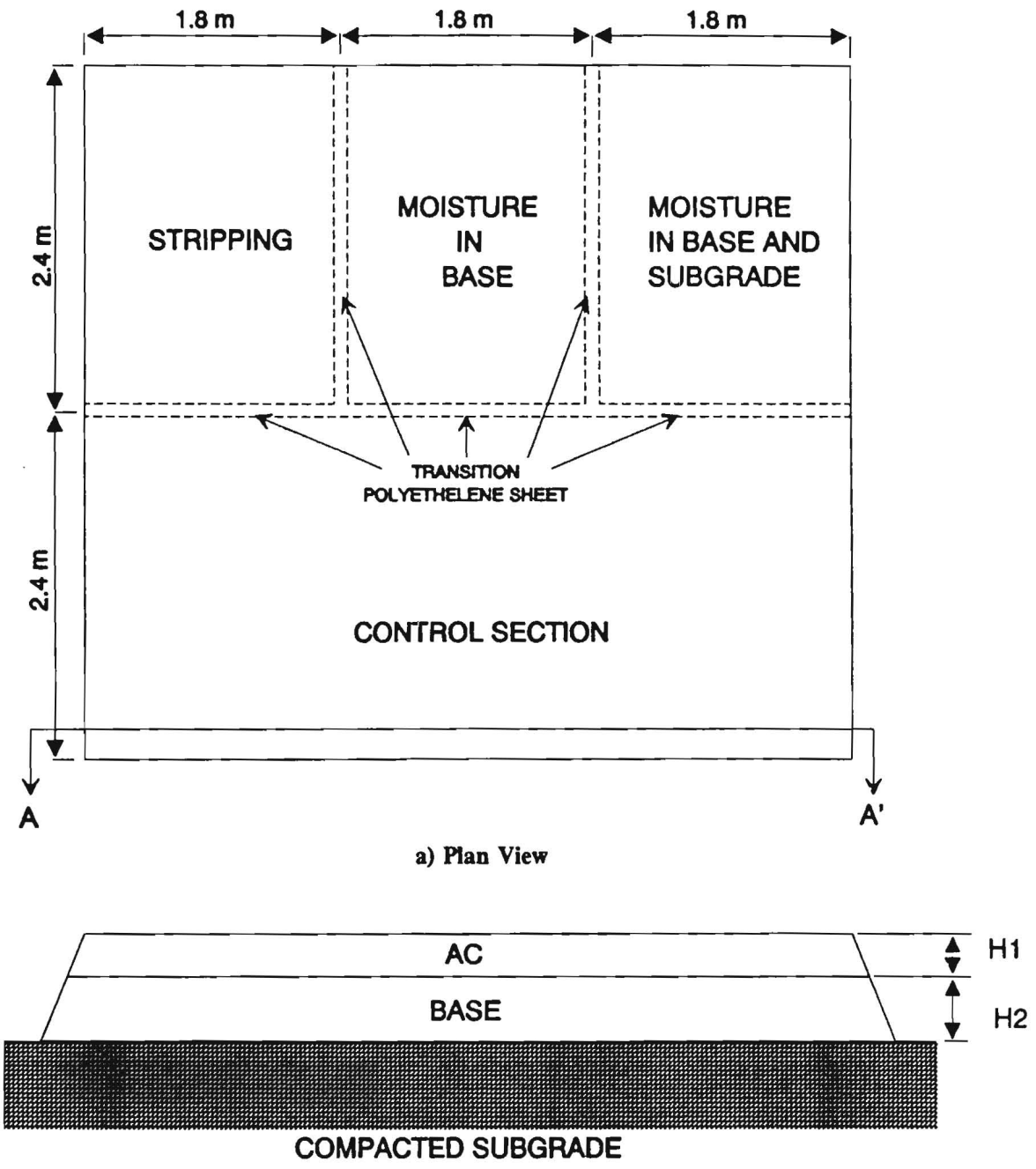

Fig. 7.4 - Schematic of UTEP flexible pavement test facility

The modulus of the AC layer was generally constant at about 4200 MPa. This is indicative of a normal AC layer. Not much variation in modulus was observed because of the small variation in the temperature (from about 18° to 23°C).

The modulus of base varies between 150 MPa for the dry condition, to about 170 MPa for the moist condition, to about 160 MPa for the saturated condition. The variation is relatively small because one sensor used in the SASW tests was located on the opposite side of the section from where the water was introduced. This resulted in dispersion curves that correspond to a region partially affected by the water and partially not. However, the variation in the modulus of the base clearly shows an increase and then a decrease in the stiffness.

Finally, the modulus of the subgrade is quite constant during the test. This is expected because the water was introduced to the base from the interface of the base and AC layer; therefore, most of the water was contained in the base layer.

The results were compared with those obtained from other impact tests (see Nazarian et al., 1993). Basically, those tests corroborate the results obtained from SASW tests.

In the second experiment, water was simultaneously introduced to the base and subgrade. The results from the SASW tests for the wet, dry, and moist conditions are summarized in Table 7.3. In the table, the moist condition also refers to the situation when the change in water content was about 7 percent. This is to make the results comparable with those obtained when water was added to the base only.

Table 7.3 - Variation in Modulus of different layers with moisture when water added to base and subgrade

Moisture Condition	Modulus, MPa		
	AC layer	Base	Subgrade
Dry	3,700	134	107
Moist*	4,117	174	117
Saturated	3,509	125	92

* Refers to the case when the change of moisture content was about 7 percent.

The modulus of the AC layer varied between 1260 MPa and 1370 MPa. Therefore, the AC modulus was not significantly affected by the change in water content. This behavior was expected, because the temperature did not vary much during these tests.

The modulus of the base layer varied — from 134 MPa in the dry condition, to a maximum of 174 MPa in the moist condition, to 125 MPa in the saturated condition. A comparison of Tables 7.2 and 7.3 reveals that the modulus of base for the dry and moist conditions are quite comparable between this experiment (where water was added to the base and subgrade) and the

previous experiment (where water was added to the base only). However, the modulus for the saturated case is lower when water was added to the base and subgrade. This may be because water was introduced at both the top and the bottom of the layer: the base layer might have been much wetter than when the water was introduced to the base only. The modulus of the subgrade is also lower when water was introduced to the base and subgrade than that when the moisture was added to the base only, for the same reasons.

The modulus of the subgrade varied from 107 MPa to 117 MPa to 92 MPa for the dry, wet, and saturated cases, respectively. Once again, the modulus increased with the moisture to a maximum, and then decreased with further moisture.

This case study demonstrates that the SASW method is effective and can successfully determine which layer or layers are most affected by a change in moisture. In addition, it has been shown that the moisture content alone is not a significant factor affecting the stiffness of a pavement section. Other factors such as the type of soil and optimum water content should also be considered.

Case Study 3

Three sections of a SPS-3 SHRP site near El Paso, Texas were tested with the SASW method to study the effects of preventive maintenance treatments on the performance of flexible pavements. The original pavement at this site consisted of 61 mm of asphalt concrete, over 213 mm of crushed-stone base and a silty subgrade. The treatments applied to the three section are AC overlay (25 mm), slurry seal (13 mm), and crack seal, respectively. The testing results are summarized in Table 7.4.

Table 7.4 - Modulus profiles obtained at a SHRP site

Section	Treatment	Modulus, MPa			Thickness, (mm)	
		AC	Base	Subgrade	AC	Base
1	Thin Overlay	6,471	258	213	67	217
2	Slurry	4,923	220	197	76	197
3	Crack Seal	5,144	203	215	59	217

The moduli of the base and the subgrade are quite close to one another. This is in character with the geology and the natural soil in the testing area.

The thickness of the AC layer varies between 60 mm and 76 mm. The thin overlay section contains a 67-mm thick AC layer, thinner than the reported value of 86 mm by SHRP. The AC layer thickness of the slurry-seal and crack-seal sections is quite close to the reported values. The thickness of the base is more or less constant at about 210 mm. This is also quite close to the thickness reported by SHRP.

FWD tests were carried out at these sections one week after the SASW tests. The deflection basins are shown in Fig. 7.5. The deflection basins vary significantly within each section. On the average, the overlaid section seems stiffest because of the lowest deflections. In contrast, the crack-sealed section yielded the highest deflections and should be the least stiff of the three sections. SASW tests were carried out at the second test point for each section.

Attempts to backcalculate the moduli failed because of the large differences between the measured and calculated deflections due to presence of caliche at shallow depths. The absolute percent sums of mismatch in deflection-basin fitting were typically about 8 percent and therefore the moduli are not presented here. The moduli of the AC layer typically tended toward the upper limit of the acceptable modulus values input to the backcalculation program. The modulus values of the base layer varied significantly. The modulus values of subgrade varied between 100 MPa and 180 MPa. In general, given the large mismatch in the basin-fitting, the values of backcalculated moduli are questionable, and they are not considered further. However, the measured deflections can be compared in a qualitative way. The trend of the deflections indicates that the stiffness of the paving layers at the thin overlay should be higher than the other two sections. The data in Table 7.4 seem to verify this interpretation.

The results from SASW tests are quite reasonable. The results are consistent with both the condition of the site and the trend of deflection from FWD deflections.

Case Study 4

Tests were carried out at a site near Atlanta. The typical pavement cross section consisted of 210 mm of AC over 250 mm of granular base over a corrodible sandy subgrade. A 1300-m section of the highway was selected and tested at 30-m intervals. The FWD device was used three weeks after the SASW tests were completed. These tests were to determine the softening of the subgrade due to the penetration of moisture. The results from the SASW tests and some information from the FWD tests are shown in Table 7.5.

The modulus of AC layers at all point tested are relatively constant. The base moduli are similar, except for points 1 and 2. In general, both AC and base layers were in good condition. The base material at points 1 and 2 was wet, and water was seeping to the pavement surface at point 1. The modulus of the subgrade were rather high for points 4 and 5, and were representative of most of the pavement section. The test point 3 corresponds to the area diagnosed as soft.

The water contents recorded in Table 7.5 were obtained in the field with a pan-dry oven. As indicated, the base at point 1 has the highest water content and also the lowest modulus. The two points 1 and 4 exhibit similar water content; however, the moduli of these two points are significantly higher than that of point 1. Point 4, with base moisture similar to point 1, is significantly stiffer than point 1. Point 1 is not as stiff as point 2 or point 4. Based on engineering intuition, the pavement structure at point 1 should therefore be softer than the other points. Points 1 and 2 are located in a rock cut, whereas point 4 was almost in a fill section.

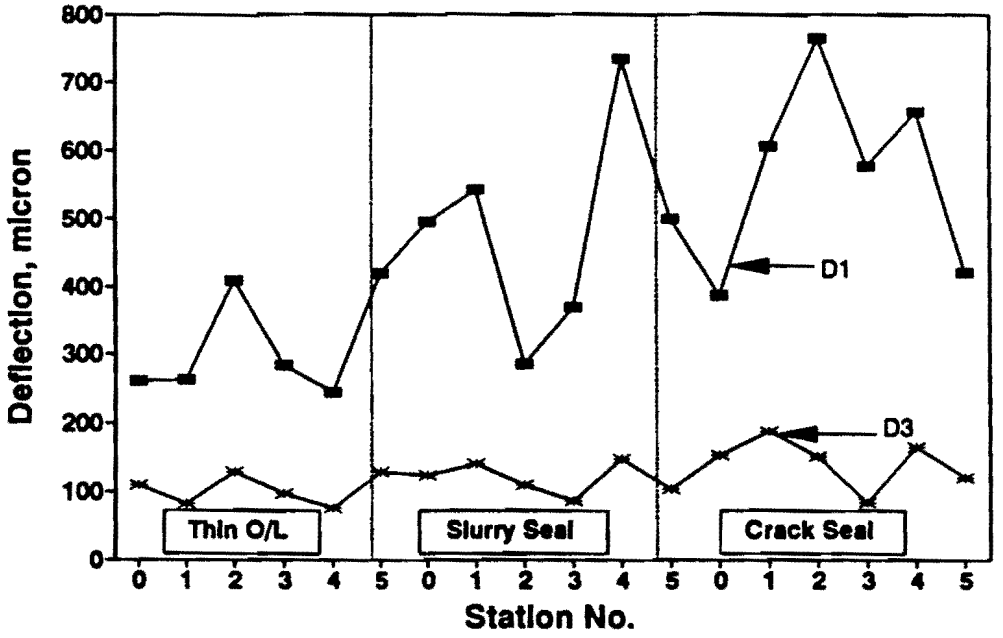

a) Sensors Close to Load

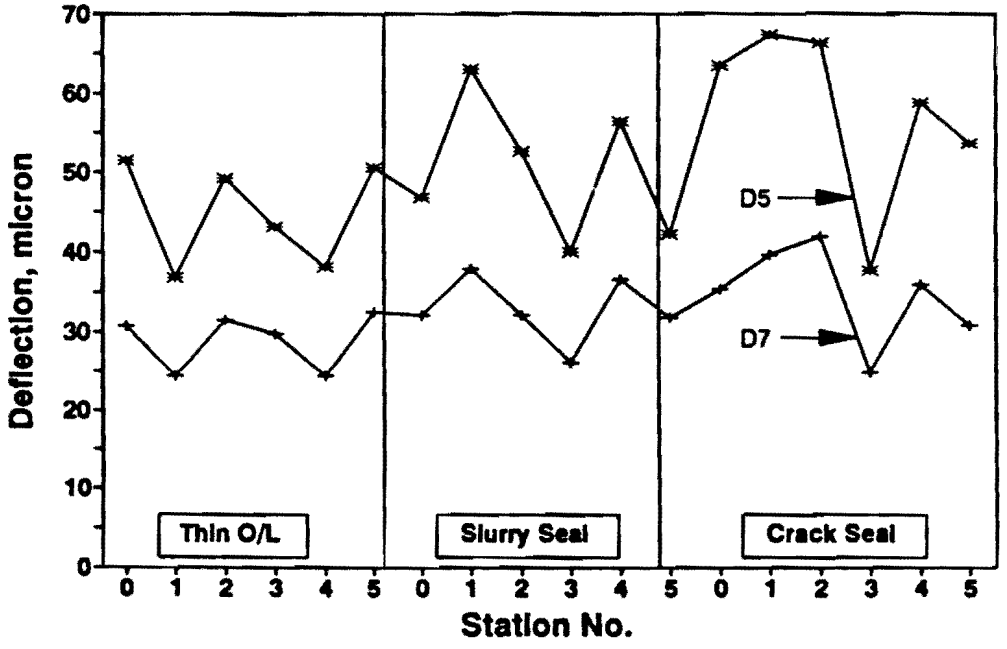

b) Sensors Far from Load

Fig. 7.5 - FWD deflection basins measured at SHRP site

In general, results from this case study clearly shows the potential, accuracy, and robustness of the SASW method. At this site, the FWD deflections could not be used for either qualitative or quantitative comparison. Backcalculation could not be carried out successfully because of the variable depth to a rigid layer in the vicinity of the pavement surface.

Table 7.5 - Modulus profiles obtained for case study 4.

Location	Modulus, MPa			Water Content, percent		FWD Deflection*, micron	
	AC	Base	Subgrade	Base	Subgrade	D1	D7
1	7,530	78	45	6.2	14.4	179**	17
2	6,433	127	89	5.7	--	182**	29
3	6,944	210	77	4.0	11.8	160	29
4	8,86	214	150	6.0	14.1	160	25
5	7,960	205	136	4.1	15.7	112	21

* Deflections, which are reported for a nominal load of 40 KN, should be considered with caution as a stiff layer existed under the pavement at variable depths.

** FWD tests were not carried out at this location, the closest point tested is reported.

Chapter 8

Summary and Conclusions

The use of nondestructive tests which are based upon wave propagation theory is increasing. The SASW method is particularly useful in determining the stiffness and thickness of the top pavement layers.

The SASW method relies on determining the stiffness (moduli) of different layers by measuring the shear wave velocity of each material. Once the shear wave velocities are known, moduli can be determined. One of the advantages of the wave propagation techniques is that fundamental material properties are measured.

In the last ten to fifteen years, most agencies that have utilized the SASW method have found it to be quite useful, and in many cases superior to other alternatives. But unfortunately, the method has been used in very limited cases. The main reasons for a lack of wide-spread use have been: 1) a lack of a rapid device for conducting these tests, 2) a lack of a robust and user-friendly software for reducing the data, and 3) a need for a highly educated and highly skilled engineer.

The seismic pavement analyzer (SPA), developed at the University of Texas at El Paso (UTEP), can easily perform SASW tests in less than one minute.

An algorithm for rapidly constructing a dispersion curve from data collected with the SPA is also developed. The algorithm is based upon fitting a complex-valued curve to the phase information of cross power spectra using coherence functions as weighting function.

Based on the general inverse theory, an inversion process for estimating layer properties of pavements from surface wave dispersion data has been developed. The theoretical principle and numerical considerations of this technique are briefly described and discussed. The limitation of the algorithm is that composite pavements cannot be interpreted.

Results from both synthetic (theoretically-derived) and actual field dispersion data are presented. These results demonstrate that the technique may be an effective tool for estimating elastic modulus profiles of pavement systems.

More work is under way to improve and accelerate the method.

References

Alsop, L. E. (1970), "The Leaky-Mode Period Equation - A Plane-Wave Approach," Bulletin of Seismological Society of America, Vol. 60, pp. 369-384.

Barker, T. G. and Stevens, J. L. (1991), "Array Processing of Rayleigh Waves for Shear Structure," Proceedings, Second International Conference on Recent Advances in Geotechnical Earthquake Engineering and Soil Dynamics, March 11-15, St. Louis, Missouri, pp. 1393-1397.

Barrodale, I. and Roberts, F. D. K. (1973), "An Improved Algorithm for Discrete L_1 Linear Approximation," SIAM Journal of Numerical Analysis., Vol. 10, No. 5, pp. 839-848.

Claerbout, J. F. and Muir, F. (1973), "Robust Modelling with Erratic Data," Geophysics, Vol. 38, pp. 826-844.

Desai, R. M. (1991), An Automated Method for Construction of Surface Wave Dispersion Curve, M.S. Thesis, The University of Texas at El Paso, 218 p.

Dobry, R. and Gazetas, G. (1986), "Dynamic Response of Arbitrary Shaped Foundations." Journal of Geotechnical Engineering, ASCE, Vol. 112, No. 2, pp. 109-135.

Draper, N. R. and Smith, H. (1981), Applied Regression Analysis, John Wiley and Sons, New York, NY, 709 p.

Drnevich, V. P., Kim, S. I., Alexander, D. R., and Kohn, S. (1985), "Spectral Analysis of Surface Waves in Pavement Systems with Random Noise Excitation," Expanded Abstracts, 55th Annual International Society of Exploration Geophysicists Meeting, Washington, D.C., October, pp. 143-145.

Dunkin, J. W. (1965), "Computations of Modal Solutions in Layered, Elastic Media at High Frequencies," Bulletin of Seismological Society of America, Vol. 55, No. 2, pp. 335-358.

Ewing, W. M., Jardetzky, W. S., and Press, F. (1957), Elastic Waves in Layered Media, McGraw-Hill, New York, 380 p.

Foinquinos, R. M. (1991), Analytical Study and Inversion for the Spectral Analysis of Surface Waves Method, Master's Thesis, The University of Texas at Austin, 187 p.

Fry, Z. B. (1965), "Dynamics Soils Investigations Project Buggy, Buckboard Mesa Nevada Test Site, Mercury, Nevada," Miscellaneous Paper No. 4-666, U.S. Army Engineer Waterways Experimental Station, Vicksburg, MS.

Golub, G. H. and Reinsch, C. (1970), "Singular Value Decomposition and Least Squares Solution," Numerische Mathemetik, Vol. 14, pp. 403-420.

Gucunski N. and Woods, R. D. (1991), "Use of Rayleigh Modes in Interpretation of SASW Test", Proceedings, Second International Conference on Recent Advances in Geotechnical Earthquake Engineering and Soil Dynamics, March, St. Louis, Missouri, pp. 1399-1408.

Haskell, N. A. (1953), "The Dispersion of Surface Waves in Multilayered Media," Bulletin of Seismological Society of America, Vol. 43, pp. 17-34.

Heisey, J. S. (1982), Determination of In Situ Shear Wave Velocities from Spectral Analysis of Surface Waves, Master's Thesis, The University of Texas at Austin, 300 p.

Hiltunen, D. R. (1988), Experimental Evaluation of Variables Affecting the Testing of Pavements by the Spectral-Analysis-of-Surface-Waves Method, Ph.D. Thesis, The University of Michigan, Ann Arbor, MI, 303 p.

Hiltunen, D. R. and Woods, R. D. (1990), "Influence of Source and Receiver Geometry on the Testing of Pavement by Surface Wave Method," Transportation Research Record, Washington, DC.

Hossain, M. M. and Drnevich, V. P. (1989), "Numerical and Optimization Techniques Applied to Surface Waves for Backcalculation of Layer Moduli," Nondestructive Pavements and Backcalculation of Layer Moduli, ASTM STP 1026, A.J. Bush III and G.Y. Baladi, Eds., American Society for Testing and Materials, Philadelphia, pp. 649-669.

Jackson, D. D. (1972), "Interpretation of Inaccurate, Insufficient and Inconsistent Data," Geophysical Journal of the Royal Astronomical Society, Vol. 28, pp. 97-109.

Jones, R. (1958), "In Situ Measurements of the Dynamic Properties of Soil by Vibration Methods," Geotechnique, Vol. 8, No. 1, March.

Jones, R. (1962), "Surface Wave Technique for Measuring Elastic Properties and Thickness of Roads: Theoretical Development," British Journal of Applied Physics, Vol. 13, pp. 21-29.

Jupp, D. L. B. and Vozoff, K. (1975), "Stable Iterative Methods for Inversion of Geophysical Data," Geophysical Journal of the Royal Astronomical Society, Vol. 42, pp. 957-976.

Kausel, E. and Roësset, J. M. (1981), "Stiffness Matrices for Layered Soils," Bulletin of Seismological Society of America, Vol. 71, No. 6, pp. 1743-1761.

Menke, W. (1984), Geophysical Data Analysis: Discrete Inverse Theory, Academic Press, Orlando, Fl, 256 p.

Miller, G. F. and Pursey, H. (1955), "On the Partition of Energy between Elastic Waves in a Semi-Infinite Solid." In Proceedings, International Conference on Microzonation for Safer Construction: Research and Application (Society of Exploration Geophysicists, Seattle, WA) Vol. 2, 545-58.

Nazarian, S. (1984), In Situ Determination of Elastic Moduli of Soil Deposits and Pavement Systems by Spectral-Analysis-of-Surface-Waves Method, Ph.D. Thesis, The University of Texas at Austin, Austin, TX, 453 p.

Nazarian S. and Desai, M. (1993), "Automated Surface Wave Testing: Field Testing," Journal of Geotechnical Engineering, ASCE, Vol. 119, No. 7, pp. 1094-1111.

Nazarian, S. and Stokoe, K. H., II (1986), "In Situ Determination of Elastic Moduli of Pavement Systems by Spectral-Analysis-of-Surface-Waves Method (Practical Aspects)," Research Report 1123-1, Center for Transportation Research, The University of Texas at Austin, 161 pages.

Nazarian, S. and Stokoe, K. H., II (1987), "In Situ Determination of Elastic Moduli of Pavements Systems by Spectral-Analysis-of-Surface-Waves Method (Theoretical Aspects)," Research Report 437-2, Center for Transportation Research, The University of Texas at Austin, 114 pages.

Reddy, S. (1992), Determination of Voids in Rigid Pavements Using the Impulse Response Method, M.S. Thesis, The University of Texas at El Paso, 201 p.

Richardson, M. H. and Formenti, D. L. (1982), "Parameter Estimation from Frequency Response Measurements Using Rational Fraction Polynomials." In Proceedings, First International Modal Analysis Conference (Society for Experimental Mechanics, Orlando, FL), 167-81.

Rix, G. J. and Leipski, E. A. (1991), "Accuracy and Resolution of Surface Wave Inversion," Geotechnical Special Publication 29.

Rix, G. J., Stokoe, K. H., II, and Roësset, J. M. (1991), "Experimental Study of Factors Affecting the Spectral-Analysis-of-Surface-Waves Method." Research Report 1123-5, Center for Transportation Research, The University of Texas at Austin, 177 p.

Rix, G. R. (1988), Experimental Study of Factors Affecting the Spectral-Analysis-of-Surface-Waves Method, Ph.D. Thesis, The University of Texas at Austin, 315 p.

Sanchez-Salinero, I., Roesset, J. M., Shao, K. Y., Stokoe, K. H., II, and Rix, G. J. (1987), "Analytical Evaluation of Variables Affecting Surface Wave Testing of Pavements," Transportation Research Record 1136, Washington, D.C., pp. 86-95.

Sansalone, M. and Carino, N. J. (1986), "Impact-Echo: A Method for Flaw Detection in Concrete Using Transient Stress Waves." Report NBSIR 86-3452, National Bureau of Standards, Gaithersburg, MD.

Satoh, T., Poran, C. J., Yamagata, K., and Rodriguez, J. A. (1991), "Soil Profiling by Spectral Analysis of Surface Waves," Proceedings, Second International Conference on Recent Advances in Geotechnical Earthquake Engineering and Soil Dynamics, March 11-15, St. Louis, Missouri, pp. 1429-1434.

Sheu, J. C., Stokoe, K. H., II, and Roesset, J. M. (1987), "Effect of Reflected Waves on SASW Testing of Pavements," Transportation Research Record 1196, Washington, D.C., pp. 51-61.

Thornhill, R. J. and Smith, C. C. (1980), "Fourier and Spectral Analysis - A Short Course," Course Notes Used for ME 397 at the University of Texas.

Uzan, J., Scullion, T., Michalek, C. H., Parades, M., and Lytton, R. L. (1988), "A Microcomputer-Based Procedure for Backcalculating Layer Moduli from FWD Data," Research Project 1123-1, Texas Transportation Institute, Texas A&M University, College Station.

Vidale, R. F. (1964), The Dispersion of Stress Waves in Layered Media Overlying a Half Space of Lesser Acoustic Rigidity, Ph.D. Thesis, The University of Wisconsin, 82 p.

Watson, T. H. (1970), A Note on Fast Computation of Rayleigh Wave Dispersion in the Multi-layered Elastic Half-Space," Bulletin of the Seismological Society of America, Vol. 60, pp. 161-166.

Willis, M. E. and Toksoz M. N. (1983), "Automatic P and S Velocity Determination from Full Waveform Digital Acoustic Logs." Geophysics, Vol. 48, No. 12, pp. 1631-1644.

Yuan, D. and Nazarian, S. (1993), "Automated Surface Wave Testing: Inversion Technique," Journal of Geotechnical Engineering, ASCE, Vol. 119, No. 7, pp. 1112-1126.